International Communications in Heat and Mass Transfer 170 (2026) 110003

Contents lists available at ScienceDirect

International Communications in Heat and Mass Transfer

journal homepage: www.elsevier.com/locate/ichmt

Impact of the turbo charging on the thermo-mechanical analysis of internal combustion engine exhaust valve'

Fatiha Sahi [a], Mahfoudh Cerdoun [a,*], Youcef Sehili [a], Mohamed Amine Elhameur [a], Lyes Tarabet [a], Carlo Carcasci [b]

[a] Laboratory of turbomachines, Ecole Militaire Polytechnique, BP17 Bordj-el-Bahri, 16046 Algiers, Algeria

[b] Department of Industrial Engineering, University of Florence, Via Santa Marta, 3, Florence, Italy.

ARTICLE INFO

Keywords:
Exhaust valves
Heat transfer
Turbocharged internal combustion engine
Thermo-mechanical stress

ABSTRACT

The valves play a crucial role in turbocharged engines by controlling the exhaust gas flow, which generates the energy required to drive the compressor and increase engine power. This paper investigates the effect of turbocharging on the heat transfer within exhaust valve, by determining the temperature distribution and mechanical stress at different engine loads and speeds, considering both naturel aspiration and turbocharged engine configurations. For this purpose, the valve is subdivided into eight adequate subdivisions to well asses the actual boundary condition surrounding the exhaust valves. The average values of the transient heat transfer coefficient, the adiabatic wall temperature and the mechanical load were evaluated at each subdivision during the engine cycle. The boundary conditionswere applied as curves defined by functions, rather thanas constant average values in order to ensure smooth transitions between subdivisions. Unsteady simulations were performed using in a finite element model implemented in ANSYS. The temperature distribution and mechanical stresses at each valve position and for divers operating condition are obtained and analyzed. The present study permit also to establish correlations to determine boundary conditions of a turbocharged engine from those of a naturally aspirated engine, allowing to quantify the thermal, the mechanical load and therefore, the new temperature map of the valves caused by the turbocharging, which could help industrial engineers to anticipate thermo mechanical variations and prevent valve overheating, thus, improving the engine's thermal efficiency, ensuring its durability, and maximizing its performance without any damage.

1. Introduction

Internal combustion engines (ICE), especially when equipped with turbochargers, generate gases at extremely high temperatures and pressures. These exhaust gases drive the turbocharger's turbine, which powers the compressor to boost intake air pressure. By increasing the intake air pressure and density, the compressor enables a greater mass of oxygen to enter the combustion chamber, resulting in more efficient fuel combustion, therefore an improved engine performance.

The rise in pressure and temperature within the combustion chamber of turbocharger engine amplify both mechanical and thermal load on the valves, especially the exhaust valves. The exhaust valves of turbocharged ICE are one of the most critical components since it manages exhaust gases at high temperatures and pressures to the turbine, which make them operating under arduous thermal and mechanical conditions [1]. These conditions push manufacturers to improve the design of

Abbreviations: Constant, -; A, Area (m^2); B, Bore diameter(m); $C_1, C_2 \ldots C_6$, Constants; C_d, Discharge coefficient; D_h, Hydraulic diameter(m); D_m, Mean valve diameter(m); D_v, valve diameter(m); D_p, Port diameter(m); D_s, Stem diameter(m); E, Young' s modulus, MPa; x, y, Coordinates; F, force (N); $F_{cam,system}$, system cam force (N); F_s, spring force (N); F_z, reaction force (N); k, thermal conductivity (W/mK); h, HTC, Height(m), Heat transfer coefficient (W/K.m^2); AWT, adiabatic wall temperature (k); k, Thermal conductivity (W/m.K), stiffness (N/m); TCC, Thermal contact conductance; L, length (m); L_v, Valve lift (m); $\dot{m}$, Mass flow; Nu, Nusselt number; P, Pressure (bar), specific pressure (N/m^2); Pr, Prandtl number; p_m, Motoring pressure; Q,q, Heat flux; R, Radial distance (m), resistance, K/W, gas constant; Re, Reynolds number; T_a, Adiabatic temperature(K); T, Temperature(K); T_{gaz}, In cylinder pressure (bar); U, Differential expansion (m); V, Volume(m^3), Velocity (m/s); V_p, Mean piston speed (m/s); V_s, Swept volume (m^3); W, Seat width; Greek symbols, ,; α, Coefficient of thermal expansion[K^{-1}], Flow angle (deg); β, Seat angle (deg); γ, Ratio of specific heats; θ, Crank angle (deg); μ, Gas dynamic viscosity (kg/m s); ε, consta nt; Subscripts, .; min, Minimum; max, Maximum; Al, Aluminum.

* Corresponding author.
E-mail address: cerdoun.mahfoudh@gmail.com (M. Cerdoun).

https://doi.org/10.1016/j.icheatmasstransfer.2025.110003

Available online 11 November 2025
0735-1933/

exhaust valves in order to avoid any failure and ensure their high performance and durability [2,3]. The exposure to high temperatures can result in material weakening, loss of hardness, and thermal expansion. Thermal stress, induced by cyclic temperature variations, which generates thermo-mechanical strains, is one of the main challenges and, over time, can precipitate cracks or fractures in different regions of the exhaust valve.

Under all these extreme thermal and mechanical loads, valves are susceptible to the geometricaldeformation which alters their geometry and affects their sealing effectiveness. Such deformation can disrupt the interface between the valve and its seat, leading to compression losses and a reduction in engine performance [4,5].An engine designer aims to achieve the optimal operating conditions that strike a compromise between maximizing engine efficiency and ensuring resistance to excessive stresses.

Prediction of heat transfer, temperature and thermal expansion through the exhaust valve requires thermal and mechanical analysis of the various valve components, which is essential to identifythe best operating parameters. Various numerical, experimental, and analytical approaches have been employed to study heat transfer within engine valves [6,7].

Early, exhaust valve surface temperatures have been measured by several researchers such as Worthen et al. [8], utilizing thermocouples placed on the valve to assess temperature at different regions.Similarly, Lai et al. [9] measured the temperature distributions on a conventional exhaust valve, and their findings revealed that the temperature in the stem_cavity part of the exhaust valve was significantly higher compared to other regions. Goudarzi et al. [10] investigated experimentally the effect of contact pressure and frequency on the heat transfer between the exhaust valve and its seat. The findings show that the thermal contact conductance (TCC) decreases as the frequency of contact increases. In the same context,Stotter et al. [11] applied two empirical equations related to the estimationof the heat transfer in the seat region. The identification of the factors that affect the development of impact stresses during the closing event of an ICE valve's was investigated by Federico et al. [12].

The main drawbacks of the previous studies are their inability to reflect the real operating conditions by disregarding actual temperature and pressure conditions, and negligence the effects of valve motion. However, due to the location of the valve and their extreme operating conditions, experimental studies are notably complex to perform.

With the progress in computational tools, researches on valves have increasingly employed numerical methods, offering a more efficient solution to the limitations of experimental studies. In this line of research, Witek et al. [13] numerically analyzed the effect of thermo-mechanical loads on the durability of exhaust valve. Therefore, Sanoj et al. [14] focus on the thermal and mechanical behavior of exhaust valves made of different materials. Zemmouri et al. [15] focused on the periodic thermal contact between the valve and its seat. Their model highlighted that transient heat transfer conditions play a decisive role in the temperature distribution and, consequently, in the mechanical stresses experienced by the valve during the engine cycle. Complementarily, Hazra et al. [16] analyzed real cases of valve failure, identifying fatigue as the main failure mechanism and demonstrating that thermal cycling accelerates crack initiation and propagation.Chavoushi et al. [17] investigated thermal stresses in exhaust valves with and without a silicon nitride ceramic coating in a diesel engine using the finite element method, showing that applying a ceramic coating significantly reduces stress, enhancing thermal resistance and extending valve lifetime. In the aim to study the effect of valves design, Deng et al. [18,19] explored the coupled thermo-mechanical behavior of four models exhaust valves to analyze and compare their responses under thermal and mechanical loads. It was found that the maximum Von Mises stress occurs primarily at the seat zone andthe maximum thermal expansion is situated on the valve head which significantly affects the maximum equivalent stress in this zone.

Knowledge of the temperature distribution within different parts of exhaust valves is essential to identify the regions of highest thermal stress. To make this possible, Woschni et al. [20] employed a correlation to estimate the averaged heat transfer coefficient (HTC) on the combustion surface, which allowed Prasad et al. [21] to conduct a transient thermal analysis of the intake and exhaust valves by segmenting the valve into five sections, whereas, Shojaefard et al. [22] employed the finite-element method to estimate the boundary conditions, and obtained the temperature distribution of the exhaust valve during the engine cycle.

Recently, Cerdoun et al. [23,24] developed a numerical model to assess the temperature map of both exhaust and intake valves, where the valve was subdivided into seven sections to evaluate the actual effect of each part separately. Consequently, the instantaneous heat transfer coefficient (HTC) and adiabatic wall temperature (AWT) were used as boundary conditions in the thermal analysis (FEM model). At different engine speed and load, Cerdoun et al. [25,26] show that the HTC increases linearly with engine speed, however, the AWT decreases slightly at partial load and increases under full engine load. In addition to the thermal load, Fersaoui et al. [27] incorporated the mechanical load and the findings highlighted that the stress intensity distribution in the zones that the part of the stem which mates with the guide, local of large temperature gradients, which causes high thermal stresses responsible of cracks or thermal fatigue damage.

Beyond valve thermal and mechanical investigations, the trend toward engine downsizing, increased specific output, and the constant pursuit of lower fuel costs remains central in current recent research achieved mainly through turbocharging [28–31]. In this context, Wang et al. [28] conducted a study on the effect of turbocharging on ICE performance by developing simulation model to predict the performance and optimize for the design parameters, whereas Zareei and al [29] investigated one-dimensional model to simulate a six-cylinder turbocharged diesel engine and the naturally aspirated diesel engine to study the effect of the turbocharger system and different fuels on the performance and exhaust emissions performance.Since a portion of the burnt gases can be recirculated through exhaust gas recirculation (EGR), which helps reduce pollution and mitigate global warming, Sehili et al. [32] investigated the improvement of efficiency and reduction of emissions in a natural gas/diesel dual fuel engine, highlighting the effectiveness of EGR in enhancing engine sustainability. Furthermore, in a complementary study, Sehili et al. [33] explored injector temperature monitoring in dual-fuel engines, demonstrating that advanced thermal analysis can provide valuable insights for optimizing combustion and controlling emissions, while Lin et al. [34] explored combustion dynamics in ammonia diesel dual fuel combustion cycles.On the other hand, Feng et al. [35] reviewed recent advances in hydrogen internal combustion engines, emphasizing mixture formation, combustion modes and abnormalities, and NOx emissions, and further summarized advanced control strategies to mitigate these challenges and improve the feasibility of hydrogen as a decarbonized alternative fuel. Additionally, the integration of a closed CO_2heat looping system with dual solid carriers in hydrogen transportation was demonstrated by Ali et al. [36] to significantly reduce cost and carbon intensity.

Although, turbochargers enhance engine performance by increasing combustion pressure and temperature, it may also lead to higher thermo-mechanical loads and can directly affect the components of the combustion chamber, particularly the exhaust valve. However, most research tends to focus on the performance improvements brought by turbocharging, without exploring its impact on heat transfer within the valves. This study aims to fill this gap by studying how turbocharging influences heat transfer in the exhaust valve. The effect is evaluated by determining the temperature distribution and mechanical stress at different engine loads and speeds, considering both with turbocharger (WT) and without turbocharged (WOT) configuration. The principal contributions of present study are summarized below, highlighting the key aspects of the study:

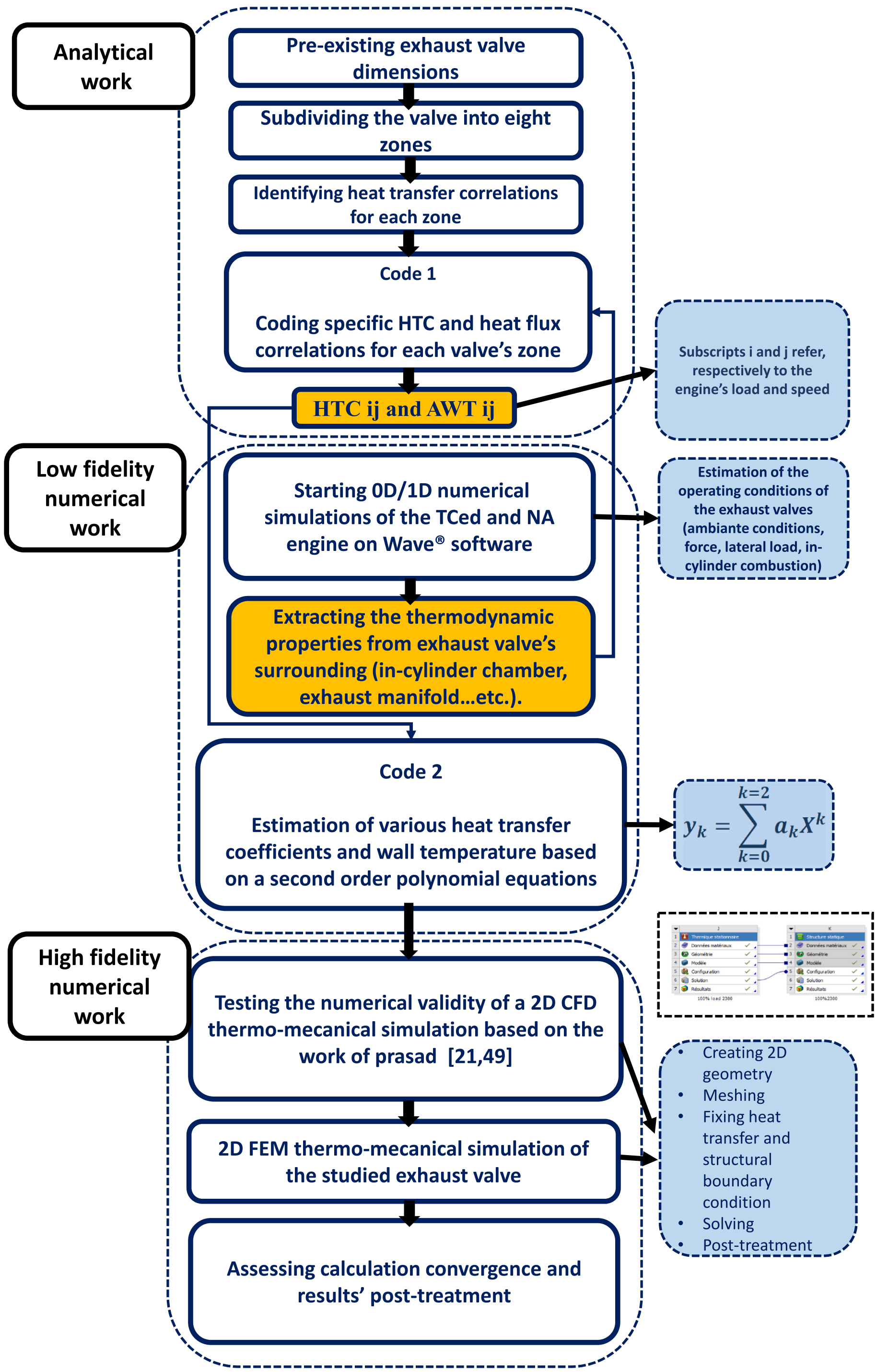

Fig. 1. Flowchart of the adopted methodology.

- Improved the numerical approach developed by Cerdoun et al. [23–27], by subdividingthe valves into eight (08) zones, in which an additional subdivision for the cavity part between the port and seat to model the curved shape is introduced, allowing better prediction of flow behavior around the valve.
- To accurately quantify the transient boundary conditions during an engine cycle, AWT and HTC boundary conditions were applied as curves (profiles) defined by functions, rather than constants average value, to ensure smooth transitions between subdivisions.
- The effect of real thermal and mechanical load conditions, considering the exhaust valve's complex surroundings, is examined through unsteady heat conduction coupled with structural analysis, under WOT and WTconfigurations of an ICE configuration.
- Establish correlations to determine the AWT and the HTC of a turbocharged engine from those of a naturally aspirated engine, for each zone of the exhaust valve, allowing toquantify the thermal, the mechanical load and therefore, the new temperature map of the valves caused by the turbocharging.

2. Numerical approach and procedure

The turbocharging has subjected the engine's components to increasingly severe thermal and mechanical conditions, particularly for

Table 1
Reynolds number formulation for the zone.

	Cylinder	Flat plat
Reynolds number	$Re_D = \frac{\rho_{gaz} V_x D_{stem}}{\mu_{gaz}}$	$Re_L = \frac{\rho_{gaz} V_y L_{stem}}{\mu_{gaz}}$
Nusseltnumber	$\begin{cases} Re_D \in [1-4000]\ a = 0.53\ b = 0.5 \\ Re_D \in [4000-40000]\ a = 0.193\ b = 0.618 \\ Re_D \in [40000-400000]\ a = 0.53\ b = 0.5 \end{cases}$	$\begin{cases} Re_D > 3\ 10^5\ a = 0.029\ b = 0.8 \\ Re_D \leq 3\ 10^5\ a = 0.664\ b = 0.5 \end{cases}$

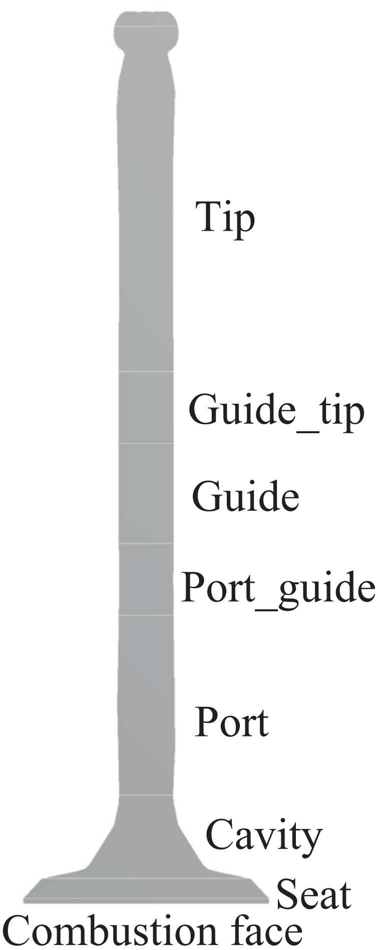

Fig. 2. Valve's subdivisions.

the exhaust valve. This has led to determine the effect of turbocharging on thermo-mechanical loadings and constraints, temperature distribution, and the maximum temperature of the exhaust valve.The followed methodology to resolve this problem is subdivided into three main steps:

a) **Analytical work:** consists on the subdividing the valves into the eight zones and the determination of mathematical formulation of the corresponding boundary conditions in term of the HTC and AWT.
b) **Low fidelity numerical work:** which starts by simulating the 0D/D1 models of the turbocharged and natural aspiration of the engine to obtain the thermodynamic parameters to be introducedinto the established formulation, where the 0D modelrepresents the in-cylinder thermodynamics (the cylinder is treated as a global control volume), and the 1D model is used to describe the intake and exhaust systems (flow properties are calculated along the ducts and manifolds). Then, the average boundary conditions are calculated for each zone and their corresponding profiles defined by functions are defined.
c) **High fidelity numerical work:** the 2D finite element method (FEM) is performed based on the estimated boundary condition, followed by the post-treatment to determine the temperature map of the valve.

The details of the overall methodology can be summarized in the flowchart of the Fig. 1. (See Table 1.)

2.1. Valve subdivisions and average boundary condition definitions

In the aim to resolve the aforementioned problematic, the actual boundary condition surrounding the ICE's valves could be well quantified by considering globally empirical correlations and the basic knowledge in both heat transfer and thermodynamics fields. In his review of empirical correlations, Finol and Robinson [37] showed that there are correlations to predict the time-averaged heat flux and the instantaneous spatially averaged heat flux, and other correlations to predict the instantaneous local heat fluxes. However, these correlations find their utilization exclusively in the combustion chamber of the ICE. For the case of valves, a proper subdivision of the valve can better simplify the tasks and it is necessary to capture the key parameters influencing heat transfer.

In the present study, the methodology adopted by Cerdoun et al. [23–27] is retained, but with enhancement of key aspects, including the number of the subdivision and the approach of how to quantify the boundary condition. The valves is subdivided in eight zones to accurately capture heat transfer phenomena and define the real arduous boundary conditions with complex surrounding geometry of engine block. This subdivision considers the different engine parts in contact with the valve (seat, stem, head), the non-uniform valve geometry, and the relative motion of the valve during the cycle. The proposed approach enables prediction of the exhaust valve temperature distribution under various operating conditions by adjusting the input parameters. Unlike previous methods, it applies transient boundary conditions linked to the crank angle and introduces an additional subdivision in the cavity region to account for exhaust gas recirculation effects. These improvements contribute to enhancing the accuracy and reliability of the results. According to Fig. 2, the considered zones are as follows:

- **Combustion Face** (Zone 1): The valve head portion in contact with the cylinder.
- **Seat** (Zone 2): The contact region between the valve and the seat.
- **Cavity** (Zone 3): the curved part with have contact with exhaust manifold.
- **Port** (Zone 4): Located in the exhaust manifold.
- **Port Guide** (Zone 5): Located intermediate between the stem port and stem guide.
- **Guide** (Zone 6): The part of the stem that engages with the guide.
- **Guide Tip** (Zone 7): Located between the stem guide and the stem tip.
- **Tip** (Zone 8): The end of the valve located in the cam system.

In ICE, the HTC is typically estimated under the assumption that the rate of heat transfer is directly proportional to the temperature difference between the fluid and the engine block, as stated by Annand [38].

The instantaneous convective heat flux $q(t)$ is expressed in **(Eq.1)**, where $h(t)$ represents the instantaneous heat transfer coefficient (HTC)

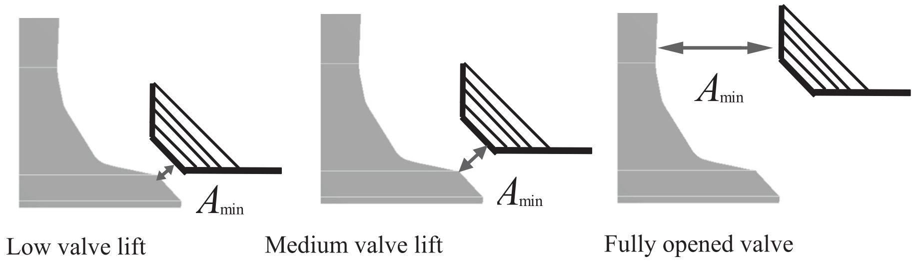

Fig. 3. Evolution of minimum flow area.

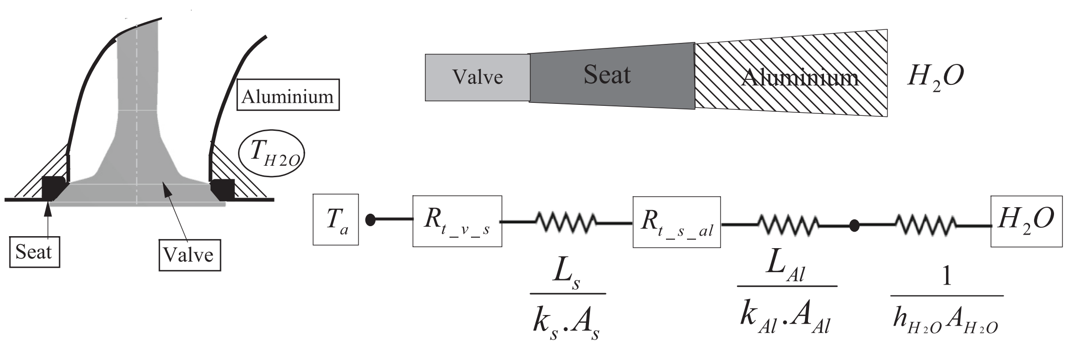

Fig. 4. Heat transfer process at closing event.

and A is the exposed surface area. $T_w(t)$ is the instantaneous wall temperature, while $T_a(t)$ corresponds to the adiabatic wall temperature (AWT), which characterizes the fluid temperature near the wall. In this study, both the unsteady HTC and the AWT are defined as functions of the engine crank angle.

$$q(t) = h(t).A[T_a(t) - T_w(t)] \tag{1}$$

From the previous equation, an average convective heat flux can be obtained:

$$\overline{q} = \overline{h}.A.[\overline{T_a} - \overline{T_w}] \tag{2}$$

Over the engine cycle period T corresponding to two revolutions of the crankshaft, the cycle-averaged convective heat flux (HTC)**(Eq.3a 3b 3c)**, and wall temperature T_w are defined by integrating their instantaneous values over the crank angle domain and normalizing by the total cycle duration.

$$\begin{cases} \overline{q} = \frac{1}{T}\int_0^T h(t).A.[T_a(t) - T_w(t)]dt \\ \overline{T_w} = \frac{1}{T}\int_0^T T_w(t)dt \\ \overline{h} = \frac{1}{T}\int_0^T h(t)dt \end{cases} \qquad \text{(3a) (3b) (3c)}$$

Whereas, the average AWT**(Eq.4)**can be derived as follows:

$$\overline{T_a} = \frac{1}{\overline{h}T}\int_0^T h(t).T_a(t)dt \tag{4}$$

2.2. Determination of boundary condition

The valve is exposedto both thermal and mechanical loads across different regions. Mechanical loads include pressure on the combustion face and stem port, reaction forces at the seat, and spring force at the top of the stem, while thermal loads consist of spatially varying heat flux in each zone.

2.2.1. Thermal boundary condition: Estimation of the instantaneous HTC

The fundamental heat transfer principles and established correlations are used to quantify these conditions at the eights valve's subdivisions.

2.2.1.1. HTC in valve combustion face. Several correlations have been developed over time to estimate the HTC in the cylinder of ICE [20,38,39]. Woschni's correlation**(Eq.5)** is selected to estimate instantaneous valve head's HTC.

$$h = 127.9\, D^{-0.2}p^{0.8}T_{gaz}^{-0.53}\left[C_1 V_p + C_2\frac{V_s T_r}{p_r V_r}(p - p_m)\right]^{0.8} \tag{5}$$

D is the cylinder bore diameter,p and T_{gaz} are cylinder pressure and temperature at each crank angle. V_p and V_s represents the mean velocity of piston ($Vp = \pi.N.D/60$) and displacement volume respectively. p_r, T_r and V_r are pressure, temperature and velocity calculated at reference state. Pm is the mean effective pressure. The constants C1 and C2 are empirically obtained.

2.2.1.2. Seat's HTC. The heat transfer at the valve seat depends on the valve position**.**

a) Opening event.

When the valve is open, the HTC of the seat zone is evaluated from the fundamental convective heat transfer equation. As described by Kastner et al. [40], the evolution of the passage area takes place in three distinct stages according to valve lift (**Fig.3**). At low valve lifts, the flow passage cross-section between the valve face and its seat forms a small, low-height truncated cone, resulting in a reduced cross-section and a highly constrained flow. As the valve opens (medium-lift), the shape of the passage becomes more complex, and the flow rate and distribution change significantly. For the both aforementioned cases, the flow is considered as internal, and the Nusselt correlation.

$$Nu = 0.023\, Re^{0.8}Pr^{0.33} \tag{6}$$

Once the valve is widely open (Fully opened valve); the flow area is

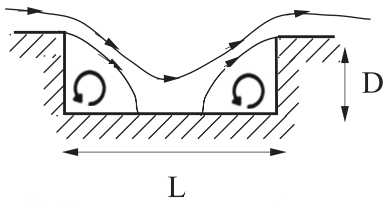

Fig. 5. Flow structure through a cavity.

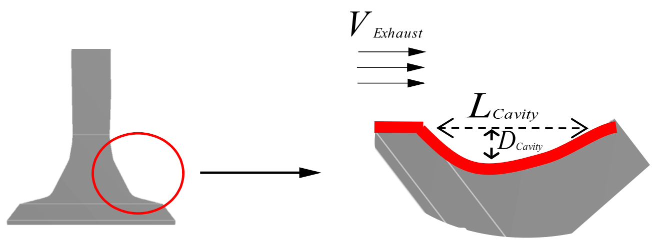

Fig. 6. Geometry specification of Cavity's zone flow area.

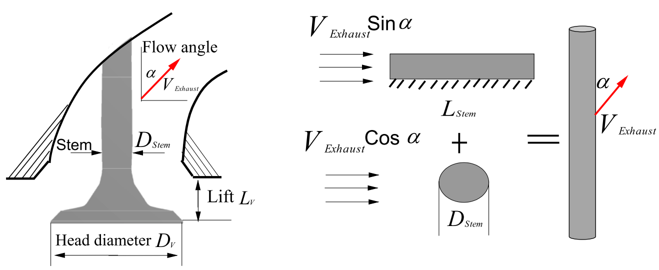

Fig. 7. Equivalent heat transfer model for inclined flow around stem zone.

considered as an annular shape. In this case the heat transfer is assumed as an external flow heat transfer over a cylinder and modeled using the Nusseltcorrelation of Churchill and Bernstein [38](**Eq.7**).

$$Nu = 0.3 + \frac{0.62Re^{1/2}Pr^{1/3}}{\left[1 + (0.4/Pr)^{2/3}\right]^{1/4}}\left[1 + \left(\frac{Re}{282000}\right)^{5/8}\right]^{-4/5} \tag{7}$$

b) Closing event.

The heat flux is transferred successively from the valve seat region, across the contact interface with the cylinder head, and then through the solid walls of the cylinder head until it reaches the cooling fluid(Fig.4). Heat transfer is modeled by an overall thermal resistance composed of five main elements includes the conduction within seat to aluminum and the convection resistance of water(**Eq.8**).

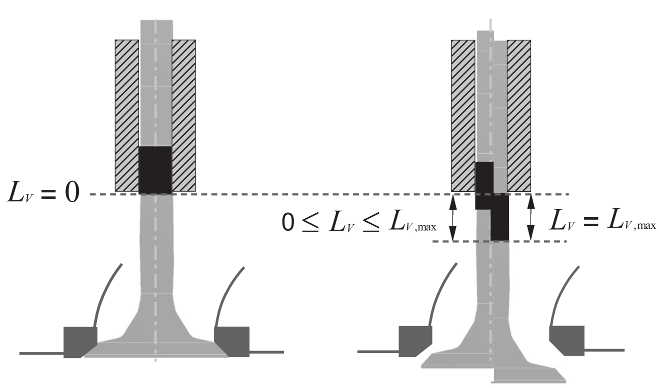

Fig. 8. Stem guide region versus valve lift.

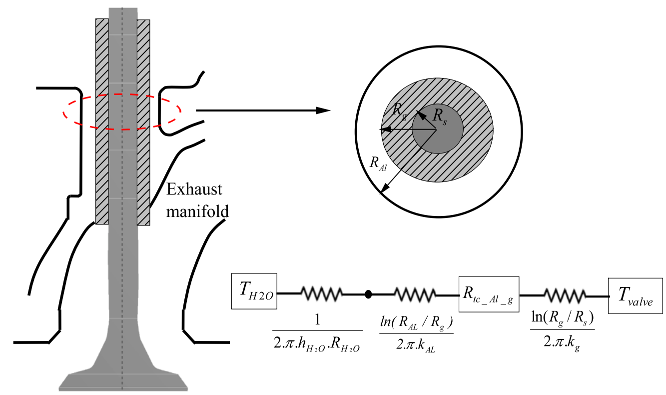

Fig. 9. Adopted heat transfer model in the stem-guide zone.

$$R_{tot} = R_{tc\_valve\_seat} + \frac{L_{seat}}{k_{seat}A_{seat}} + R_{tc\_seat\_Al} + \frac{L_{Al}}{k_{Al}A_{Al}} + \frac{1}{h_{H_2O}A_{H_2O}} \tag{8}$$

A_{seat}, A_{Al} and A_{H_2O} correspond to the cross-sectional areas, shaped like a truncated cone, for heat transfer through the valve seat region, the aluminum section of the engine block, and the cooling system, respectively. The length L_s and L_{al} refer to the material thicknesses of the valve seat and the aluminum section.

The estimation of the thermal contact conductance (TCC) between the valve and the seat, as well as between the seat and the aluminum cylinder head, directly affects the accuracy of the overall thermal resistance calculation [25]. Numerous researchers have investigated this issue from both theoretical and experimental perspectives. Among them, Song andYovanovich [41] provided in-depth analysis by incorporating parameters such as Vickers hardness and contact pressure into their correlations.

2.2.1.3. HTC in the cavity subdivision. Heat transfer in cavities depends on both the flow regime and the cavity geometry including its depth, length in the flow direction, and aspect ratio which governs the development of recirculation zones and thermal gradients that affect the exchange between the fluid and the cavity walls (Fig.5).

One of the significant experimental studies on cavity heat transfer was conducted by Yamamoto et al. [42]. They investigated the effect of downstream wall height variations on heat transfer characteristics, showing that vortex flow inside the cavity significantly depends on the aspect ratio and main flow velocity. Furthermore, many studies have focused numerically on laminar flows in deep cavities [43–45]; for instance, Bhatti et al. [43] and Aung [44]. In turbulent regimes, Richards et al. [45] established a correlation linking the Nusselt number (based on cavity height) to the Reynolds number, showing that the heat transfer rate is predominantly determined by the cavity's aspect ratio.According to Chapman's model [46], which treats the cavity as an isothermal region of stagnant air, heat transfer in laminar flow is lower than that in an attached flow, while in turbulent flow it varies with the Reynolds number.

In this article the cavity valve's part is modeled using Yamamoto's correlation, which provides a wide range of valuable correlations for heat transfer in cavities with varying wall heights. This correlation covers the data corresponding to our configuration which ensure a modeling approach adapted to the specific conditions of our analysis, considering both aspect ratio (Fig.6).and flow regimes (**Eq.9**) and (**Eq.10**).

-Laminar flow

$$\begin{cases} Re_L \geq 0.75\,10^4 \\ Nu_L = 0.39\,Re_L^{\frac{1}{2}}\left(\frac{D_{Cavity}}{L_{Cavity}}\right)^{-0.27} \end{cases} \tag{9}$$

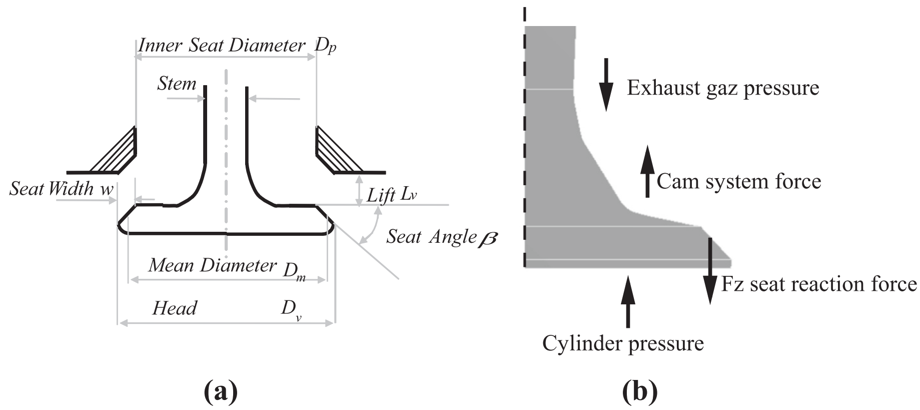

Fig. 10. (a) valve geometry (b) Equilibrium forces acting on the valve at closing event.

- Turbulent flow

$$\begin{cases} Re_L < 0.75\ 10^4 \\ Nu_L = 0.427\ Re_L^{\frac{1}{3}} \end{cases} \tag{10}$$

2.2.1.4. Port's HTC. Heat transfer in the valve port is modeled by applying the fundamental principles of turbulent flow around a cylinder, using empirical correlations to estimate the Nusselt number. Since the exhaust gas flow is inclined due to the orientation imposed by the exhaust manifold(Fig.7), Carcasci et al. [47] modeled the heat transfer as the combination of two components(**Eq.11**): one perpendicular to the valve port region, treated as crossflow around a cylinder, and another parallel to the surface, treated as flow along a flat plate.

$$h_{stem\_port} = h_{cylinder} + h_{flatplat} \tag{11}$$

(See Fig. 8

The Nusselt number is calculated using Churchill and Bernstein correlation [48]$Nu_D = 0.43 + a\ Re_D{}^b Pr^{0.31}$, While for a flat plat, the Nusselt number is estimated as $Nu = a\ Re^b Pr^{0.33}$ where the coefficients a and b are determined according to the flow regime around a cylinder and flat plat, summarizing in the **Table 1**.

2.2.1.5. Guide_port's HTC. When the valve is closed, this section is in direct contact with the guide, and the heat transfer is governed by the guide's HTC. As the valve lift increases, this section gradually enters the exhaust port, and the heat transfer of the port starts to contribute; until it becomes fully exposed to the exhaust manifold at maximum lift **(Eq.12)** ($HTC_{\text{stem\_guide}}$ when $Lv = 0$, $HTC_{\textbf{stem\_port}}$ at $L_v = L_{v,Max}$, and an average in between)(Fig. 8).

$$HTC_{\mathbf{s-g/p}} = \left(\frac{L_{v,Max} - L_v}{L_{v,Max}}\right) HTC_{\mathbf{s-g}} + \left(\frac{L_v}{L_{v,Max}}\right) HTC_{\mathbf{s-p}} \tag{12}$$

2.2.1.6. Guide's HTC. The heat transfer in the stem–guide region is modeled as radial conduction through a multilayer cylindrical assembly. Heat is transferred from the stem–guide zone of the valve to the cooling system, traversing a series of layers: the lubricating oil film, the guide, and the aluminum of the engine block(Fig.9). The total thermal resistance **(Eq.13)**is expressed following the methodology of [22–25].

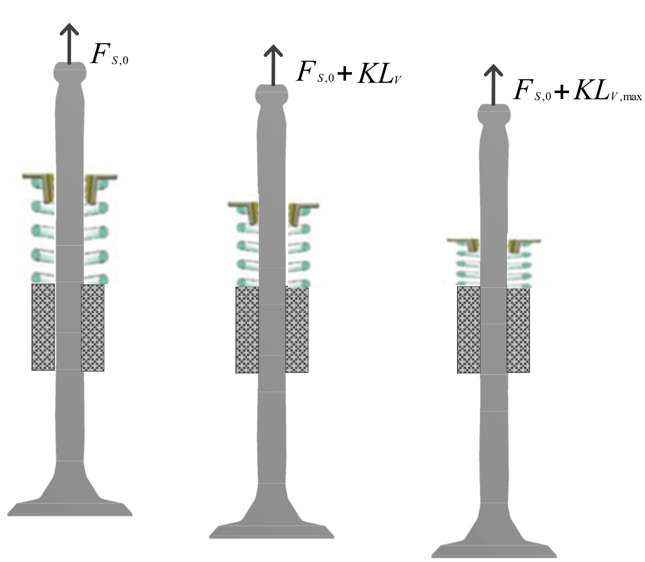

Fig. 11. Spring force versus valve.lift.

Table 2
Average mechanical boundary condition.

	Zones	Mechanical
01	***Combustion face***	$\overline{P_{cylindr}} = \frac{1}{T}\int_0^T P_{Cylinder}(t)dt$
02	***Seat***	$\overline{P_{seat}} = \frac{1}{T_{close}}\int_0^{T_{close}} P_{seat}(t)dt + \frac{1}{T_{open}}\int_0^{T_{open}} P_{Cylinder}(t)dt$ $Fz = \frac{1}{T}\int_0^T Fz(t)dt$
03	***Cavity***	$\overline{P_{port}} = \frac{1}{T}\int_0^T P_{port}(t)dt$
04	***Port***	$\overline{P_{Cavity}} = \frac{1}{T}\int_0^T P_{Cavity}(t)dt$
05	***Port-Guide***	$\overline{P_{port\_guide}} = \frac{1}{T}\int_0^{T_{close}} P_{port\_guide}(t)dt$
06	***Guide***	/
07	***Guide-Tip***	$\overline{F_{Spring\_guide\_tip}} = \frac{1}{T}\int_0^{T_{close}} F_{Spring}(t)dt$
08	***Tip***	$\overline{F_{Spring}} = \frac{1}{T}\int_0^T F_{Spring}(t)dt$

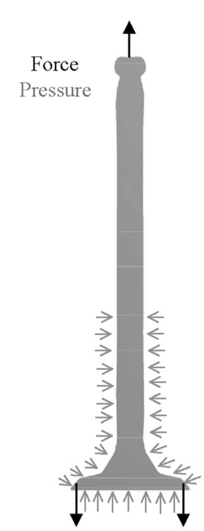

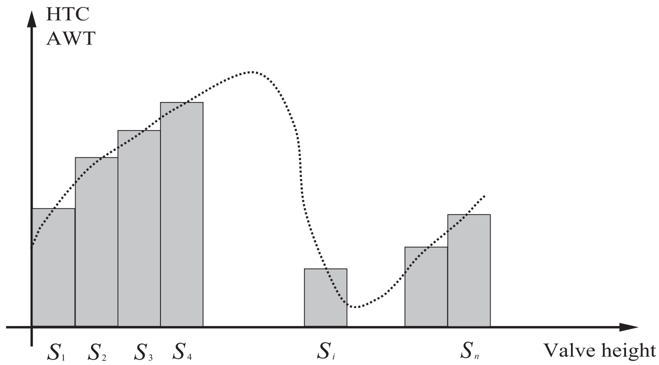

Fig. 12. Illustration of the smooth transition between zones.

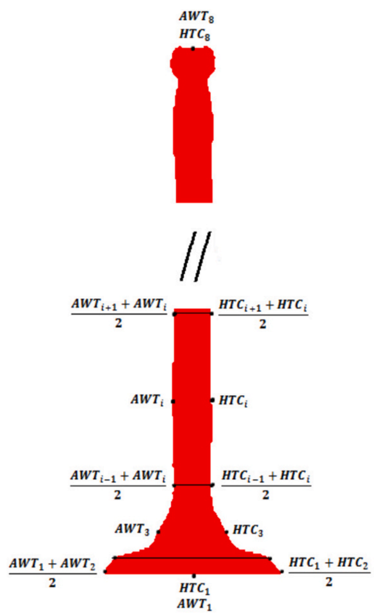

Fig. 13. Illustration of the boundary conditions, considering the effect of the adjacent zones (i-1) and (i + 1) on zone (i).

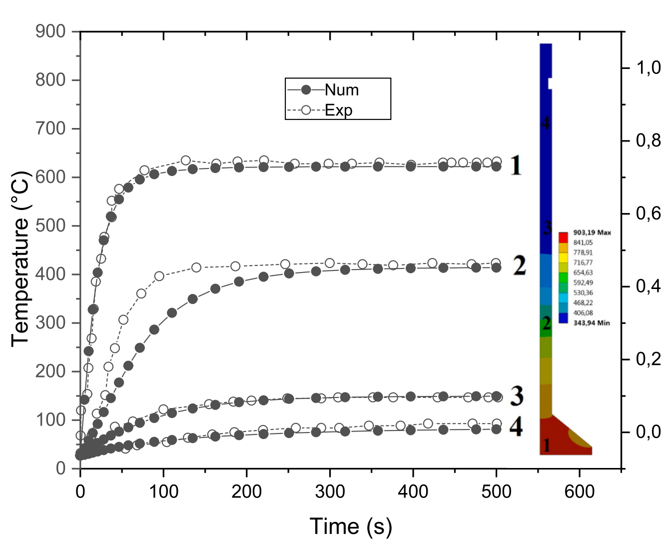

Fig. 14. Comparison between the simulation results and the experimental data.

Table 3
Aspects and factors guiding the present methodology and improvements upon previous approaches.

Aspect	Rationale & Advantage	Key Example / Outcome
1. Surrounding Components	The valve contacts different engine parts, each imposing unique boundary conditions. Subdivision allows precise application of the correct physical model for each interface.	**Zone 1 (Combustion Face):** Uses cylinder-specific HTC (Woschni correlation). **Zone 2 (Seat):** Switches between conduction (valve closed) and convection (valve open) models.
2. ComplexGeometry	The valve's non-uniform shape creates vastly different local flow and heat transfer phenomena. Fine subdivision prevents averaging errors and captures these critical details.	**Zone 3 (Cavity) vs. Zone 4 (Port):** The curved cavity (recirculating flow) and cylindrical port (duct flow) require distinct models (Yamamoto vs. Churchill-Bernstein correlations).
3. Valve Motion	The valve's movement changes its interaction with gases and components throughout the cycle. Subdivision accounts for these transient effects on heat transfer type and intensity.	**Zones 5 & 6 (Port/ Guide):** The HTC is a weighted average based on valve lift, as these zones transition between being exposed to the port or covered by the guide.
4. EnhancedResolution	Provides a high-fidelity map of fluid dynamics and heat transfer, capturing gradients that are smoothed over in models with fewer, larger zones.	Prevents inaccuracies from generalizing disparate regions (e.g., grouping the hot cavity with the cooler port).
5. SmoothBoundary Condition Transition	The detailed zones enable defining HTC/AWT as **spatially-varying functions** (Eq. 18), not constant values. This eliminatesunphysical jumps at zone interfaces.	Results in a continuous and realistic distribution of boundary conditions (Fig. 12), a significant improvement over prior work.
6. ImprovedAccuracy	The combined effect of the above points is a more realistic foundation for the simulation, directly leading to more reliable predictions of temperature and stress.	Validation against experimental data (Fig. 14) showed very good agreement, confirming the model's reliability and the value of this approach.

Table 4
Valves head and geometrical parameters.

Parameters	Values
Seat length	4.20 mm
Mean stem diameter	7.94 mm
Mean valve diameter	29.57 mm
Maximum lift	8.41 mm
Valve length	112 mm
Seat angle	45°

$$R_{eq} = \frac{1}{2\pi R_{al} h_{H_2O}} + \frac{\ln\left(\frac{R_{al}}{R_g}\right)}{2\pi k_{al}} + R_{tc-al-g} + \frac{\ln\left(\frac{R_g}{R_S}\right)}{2\pi k_g} + R_{Oil} \tag{13}$$

2.2.1.7. Guide tip'sHTC. Along the valve's operating cycle, this region is alternately subjected to the thermal conditions of both the guide and the tip, depending on the valve lift. The same way as stem-guide/port zone is used to obtain the instantaneous guide_tip's HTC; thus, an effective HTC(**Eq.**14) is computed as a weighted average between the stem-guide and stem-tip values.

Table 5
Diesel engine specifications [50].

Components	Value
Engine type	6 Cylinders, 5.9 l (4-strokes)
Horsepower	200 kW @ 2500 rpm
Torque	1000 N.m @ 1250 rpm
Bore x Stroke	102 mm × 120 mm
Aspiration	Turbocharger and intercooler
Firing order	1–5–3-6-2-4
Valve train	4 Valves per a cylinder
Compression ratio	17

$$HTC_{\mathbf{s-g/t}} = \left(\frac{L_{v,Max} - L_v}{L_{v,Max}}\right) HTC_{\mathbf{s-t}} + \left(\frac{L_v}{L_{v,Max}}\right) HTC_{\mathbf{s-g}} \quad (14)$$

2.2.1.8. Tip's HTC. The spring in the camshaft system ensures that the valve closes properly and remains in contact with the actuation mechanism throughout the cycle. The tip of the valve stem directly exposed to air, exchanges heat with the surrounding environment. It is therefore reasonable to model the heat transfer in this zone using a constant convection coefficient equivalent to that of air.

2.2.2. Mechanical boundary condition

The mechanical loading conditions are established based on the

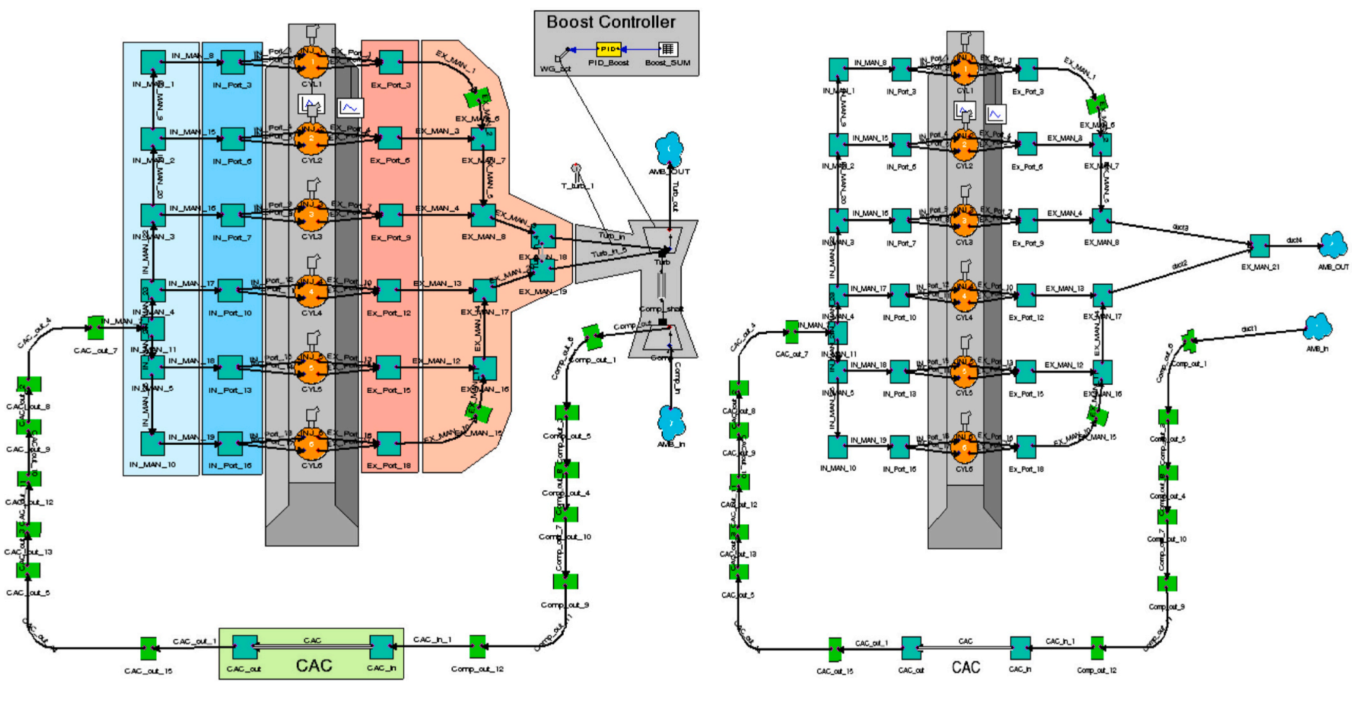

(a) (b)

Fig. 15. 1D wave model for a Turbocharged (a) and a Naturally aspirated engine(b).

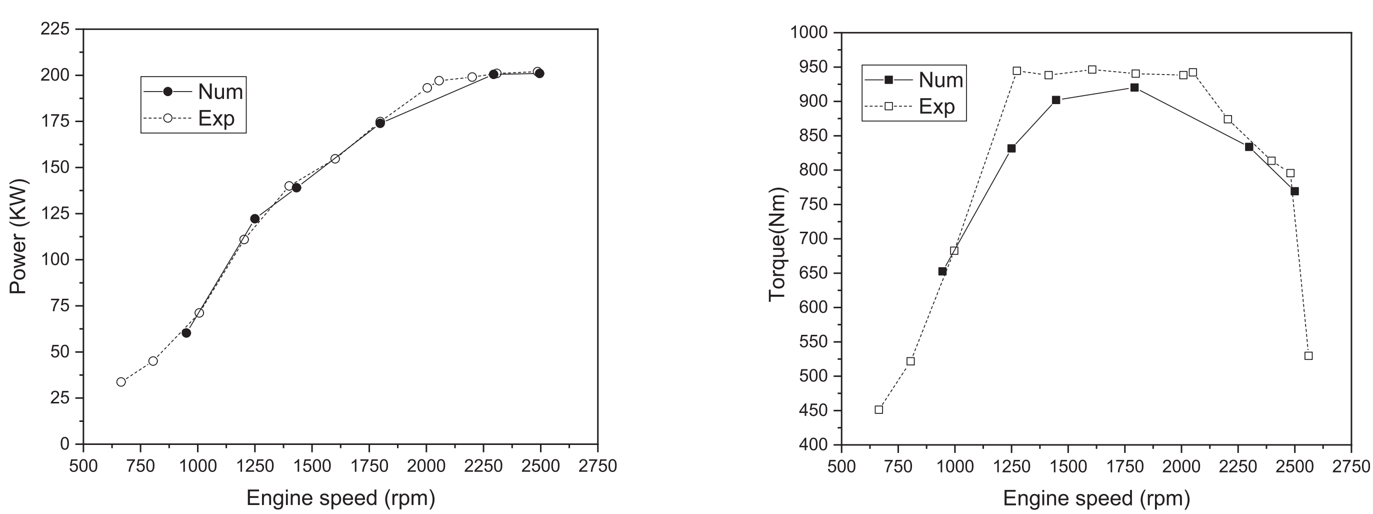

(a) (b)

Fig. 16. Experimental validation of the 1D wave model in terms of power (a) and torque (b).

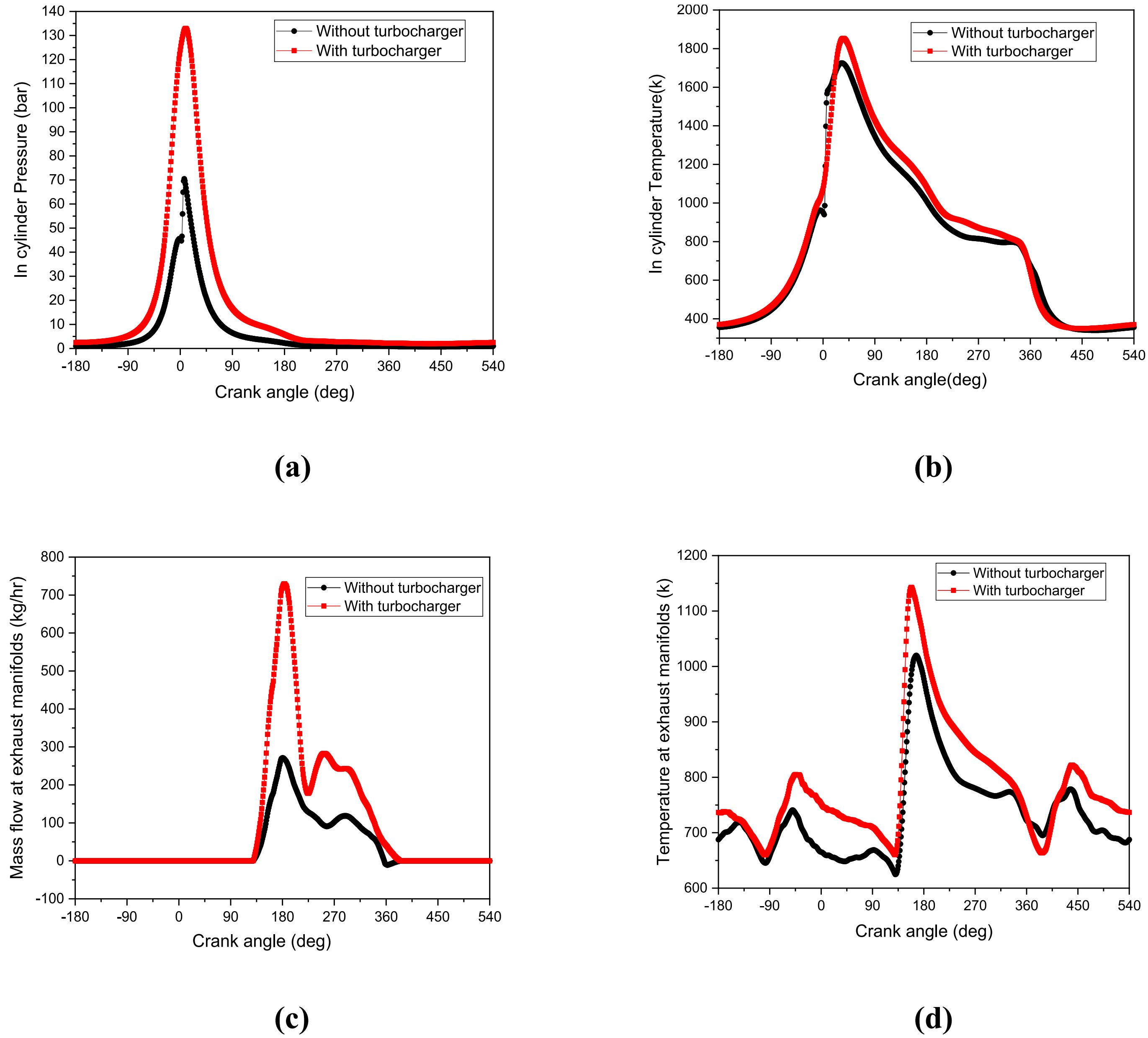

Fig. 17. Evolution of the thermodynamic parameters in term of (a) pressure cylinder, (b) Temperature cylinder, (c) Mass flow rate at the exhaust manifolds and (d) Exhaust gases temperature.

average load over a complete engine cycle. The pressure distribution acting on the valve combustion face, valve port, and valve cavity is determined by integrating the instantaneous pressure at each time step throughout the cycle. This approach captures the dynamic variations in pressure and force, ensuring an accurate representation of the loading conditions.

In practice, the dynamic pressure from combustion gases, the pressure of exhaust gases, and any additional mechanical loads must be balanced by the reactive force from the valve seat, ensuring force equilibrium. Based on this, Newton's first law is applied to determine the contact pressure P and the force exerted at the valve seat when the valve is closed, considering the equilibrium forces acting on the valve **(Fig. 10)**.

With the reaction force Fz and the contact pressure $P_{seat-contact}$ at the seat are expressed in **(Eq.15)**and **(Eq.16)** respectively.

$$Fz = \left(\pi \frac{D_v^2}{4}\right) P_{cylindre} + F_{cam,sys} - \frac{\pi}{4}\left(D_p^2 - D_s^2\right) P_{port} \tag{15}$$

$$P_{seat-contact} = \frac{Fz}{\frac{\pi}{4}\left(D_v^2 - D_p^2\right)} \tag{16}$$

Where D_v, D_s and D_p are shown in**(Fig. 10a).**

The pressure P_{guide_port}**(Eq.17)** applied on the guide port is equivalent to the exhaust gas pressure when the valve is open.

$$P_{guide\_port} = \left(\frac{L_{v,Max} - L_v}{L_{v,Max}}\right) P_{guide} + \left(\frac{L_v}{L_{v,Max}}\right) P_{port} \tag{17}$$

During the installation of the cam system, the valve spring is initially compressed to ensure effective valve closure, exerting an initial force $F_{s,0}$ before any occurring movement. As the valve begins to open**(Fig.11)**, the spring is further compressed, causing the spring force to increase proportionally with the valve lift. This behavior is governed by Hooke's law, which states that the spring force grows linearly with displacement from its initial position. As a result, the total spring force acting on the valve during its opening can be expressed using **(Eq.18)**.

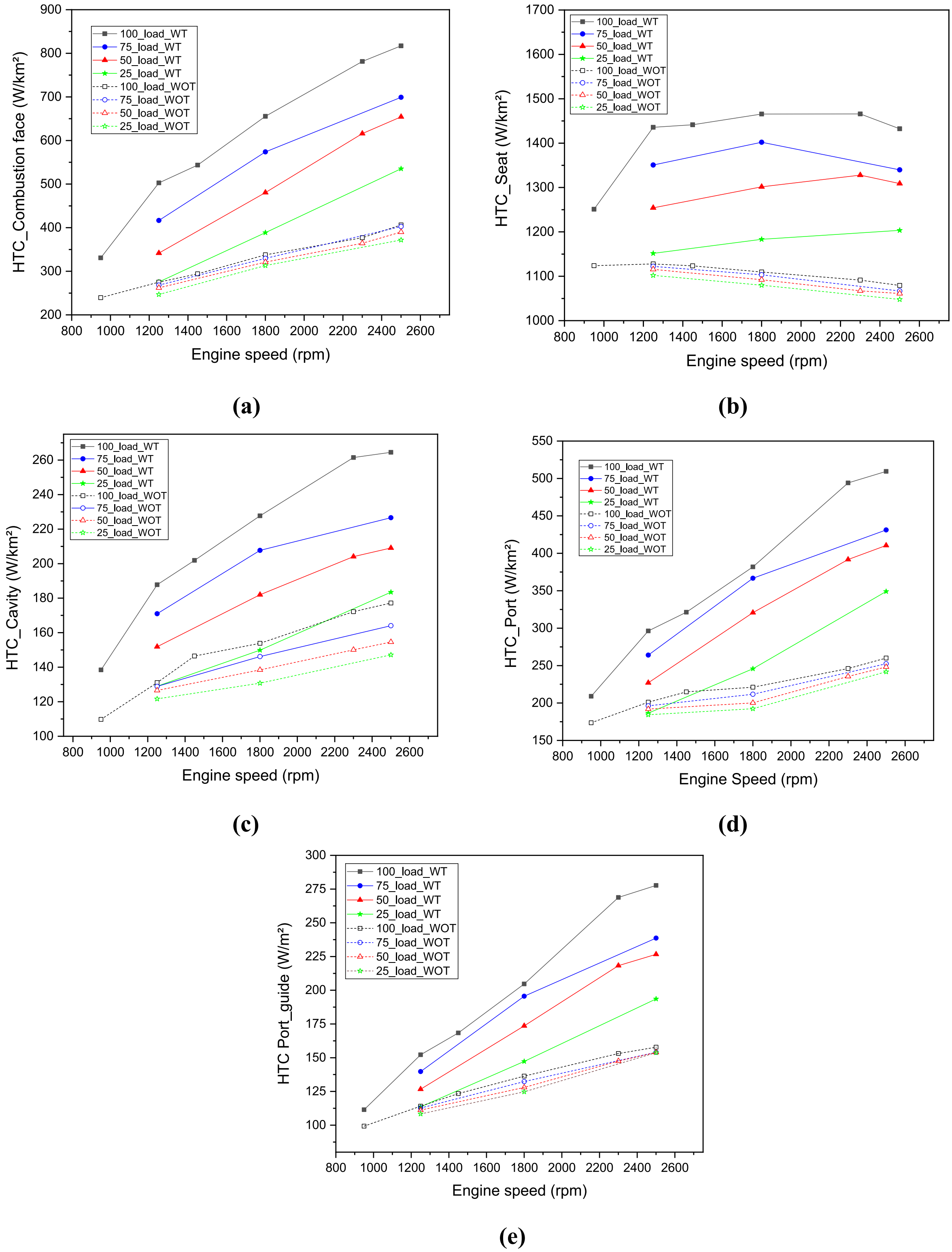

Fig. 18. Averaged HTC versus engine speed for (a) combustion face, (b) seat, (c) cavity, (d) port and (e) port/guide zone.

$$F_{Spring} = F_{s,0} + KL_v \tag{18}$$

K is the spring constant, which characterizes the stiffness of the spring. The maximum valve lift corresponds to the point where the spring is compressed to its maximum displacement, generating the peak spring force.

Basing on the aforementioned assumption the mechanical load on each zone is summarized in Table 2. (See Tables 3 and 4.)

2.3. Quantification of the boundary conditions

For the thermal modeling of the valve, previous studies have generally relied on the application of constant boundary conditions in each subdivision [23–27]. In reality, the transition between these zones is not discontinuous. Thermal and fluid dynamic conditions in each zone are affected not only by local properties but also by interactions with

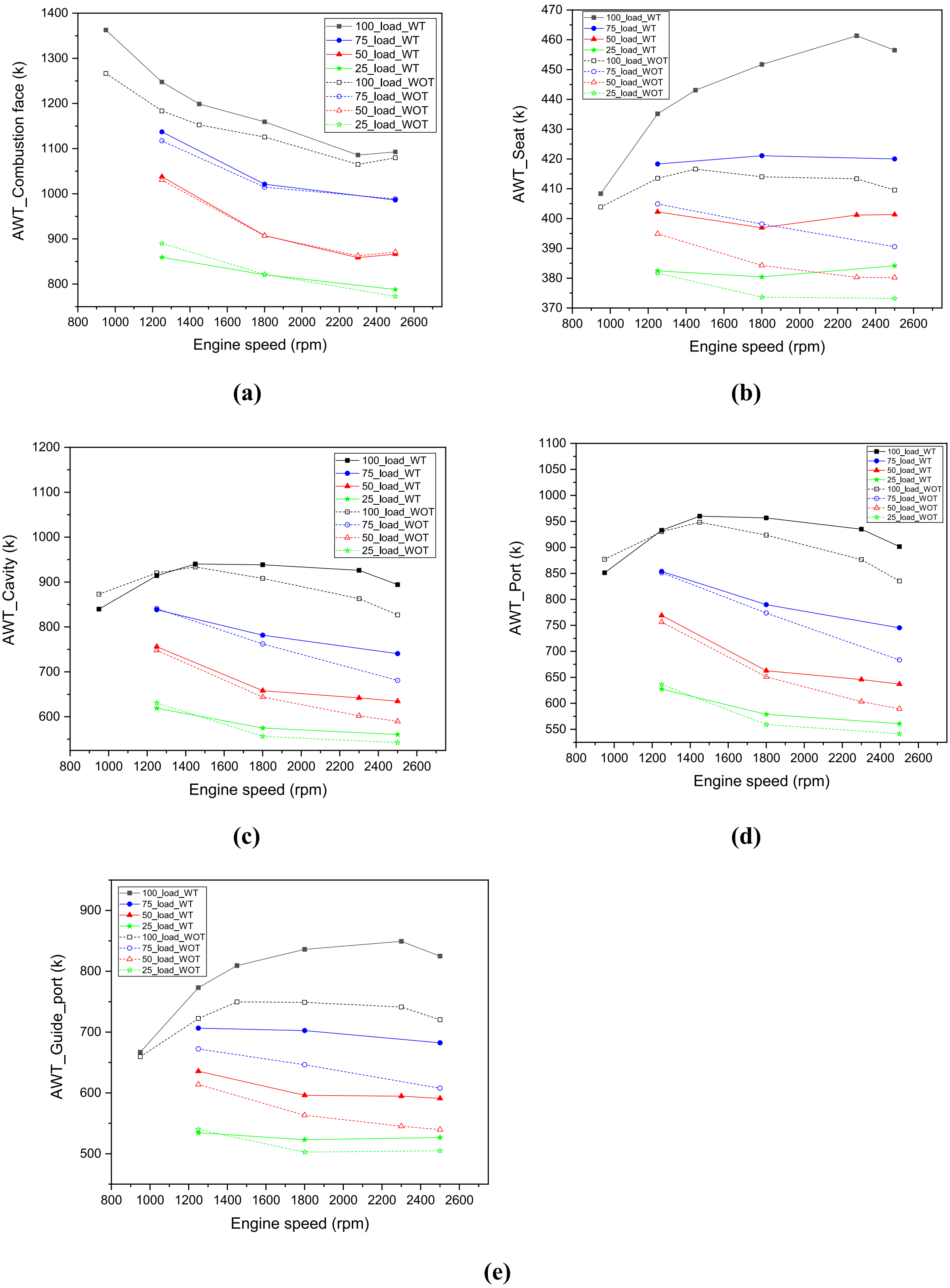

Fig. 19. Averaged AWT versus engine speed for (a) combustion face, (b) seat, (c) cavity, (d) port and (e) port/guide zone.

adjacent zones.

It is therefore crucial to smooth the transitions between the different zones of the valve to achieve realistic boundary condition. To quantify the boundary conditions on the different valve zones instead of using constant average values, AWT and HTC variations were modeled as curves defined by polynomial functions of second order in the form of $y = ax^2 + bx + c$. This method ensures a gradual transition between zones and greater consistency in the modeling as represented in the (Fig.12) in term of HTC and AWT defined spatially in **(Eq.19)**.

$$\begin{cases} HTC_i(x) = a_i x^2 + b_i x + c_i \ldots\ldots(1) \\ AWT_i(x) = aa_i x^2 + bb_i x + cc_i \ldots\ldots(2) \end{cases} for\ \mathrm{i} = 1\ldots8 \tag{19}$$

(See Fig. 13.)

To determine the coefficients of these polynomials functions ($\sum_{i=1}^{8} a_i$, $\sum_{i=1}^{8} b_i$, $\sum_{i=1}^{8} c_i$), it was imposed that the polynomial function

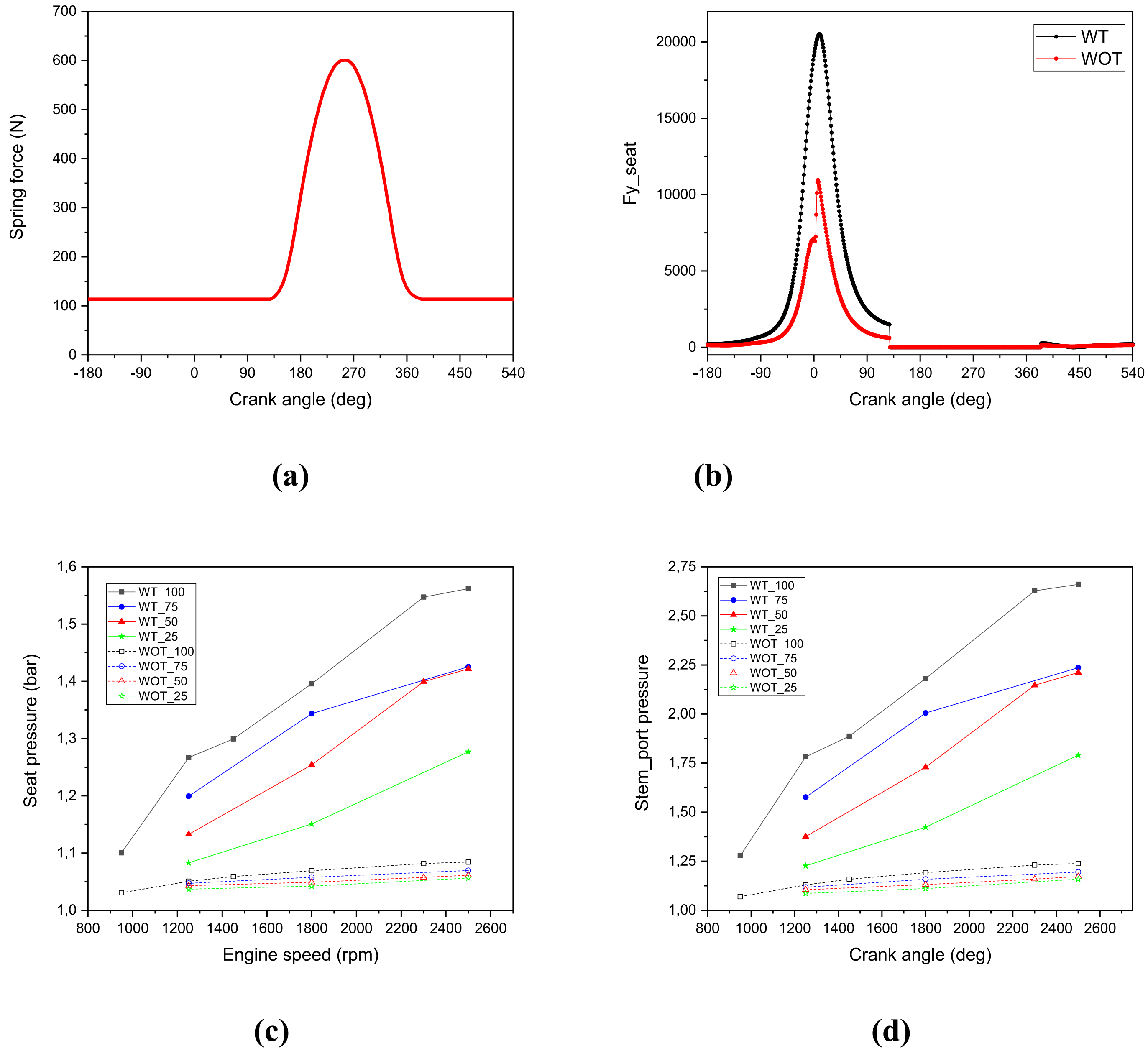

Fig. 20. Mechanical boundary conditions: (a) Instantaneous spring force, (b) Instantaneous seat reaction force, (c) Average seat pressure versus engine speed and (d) Average port pressure versus engine speed.

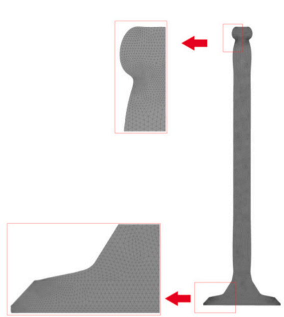

Fig. 21. Valve mesh.

passes through three well-defined points of the function such as midpoint and the two extremities of each subdivision. This selection considers the effect of the adjacent zones $(i-1)$ and $(i+1)$ on zone (i) (Fig. 13).

Therefore, the system $A_i x = B_i$ is solved for each subdivision and for equation **(Eq.20)** and **(Eq.21)**using the vector B_i defined for HTC's and AWT's respectively.

$$\begin{cases} B_i = \left[HTC_i; \dfrac{HTC_{i-1} + HTC_i}{2}; \dfrac{HTC_{i+1} + HTC_i}{2}\right] \text{ for i} = 2\ldots7 \\ B_i = \left[HTC_i; \dfrac{HTC_i + HTC_{i+1}}{2}; \dfrac{HTC_i + HTC_{i+1}}{2}\right] \text{ for i} = 1 \\ B_i = \left[HTC_i; \dfrac{HTC_{i-1} + HTC_i}{2}; \dfrac{HTC_i + HTC_i}{2}\right] \text{ for i} = 8 \end{cases} \tag{20}$$

Table 6
The mains results of GCI approach.

	Mesh number	Grid size	h_i	r_i	f_i	P	$f_{h=0}^{i,i+1}$	$e_r^i(\%)$	$e_{ext}^i(\%)$	$GCI_{ext}^i(\%)$
	1	32,773	1.9 10^{-4}	0.67	942.58	−1.94	942.55	3.18 10^{-5}	2.72 10^{-5}	0.00341
T_{Cyl}	2	14,753	2.8 10^{-4}	0.51	942.61				5.90 10^{-5}	0
	3	3829	5.5 10^{-4}		942.73				1.86 10^{-4}	
	1	32,773	1.9 10^{-4}	0.67	814.64	−2.36	814.56	1.47 10^{-4}	9.40 10^{-5}	0.0117
T_{Seat}	2	14,753	2.8 10^{-4}	0.51	814.76				2.41 10^{-4}	0
	3	3829	5.5 10^{-4}		815.35				9.65 10^{-4}	

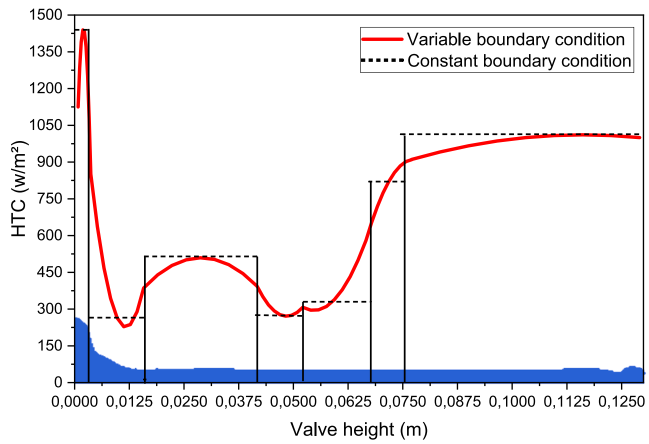

Fig. 22. HTC's profil versus constant HTC applied on valve.

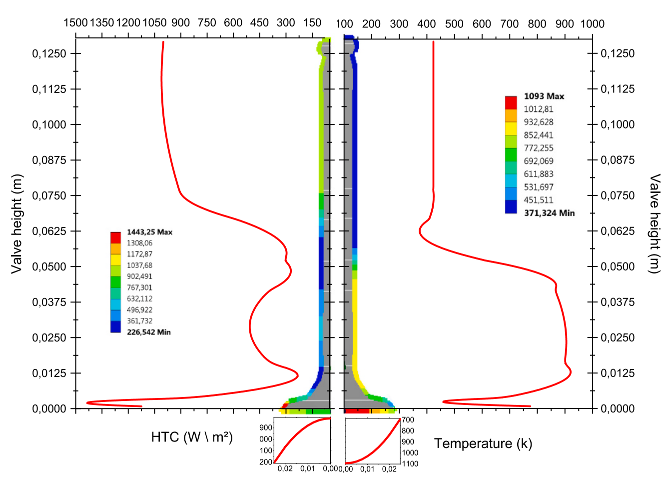

Fig. 23. Spatial evolution of variable boundary conditions applied to the valve (HTC on the left and AWT on the right).

$$\begin{cases} B_i = \left[AWT_i; \dfrac{AWT_{i-1} + AWT_i}{2}; \dfrac{AWT_{i+1} + AWT_i}{2}\right] \text{ for i} = 2\ldots7 \\ B_i = \left[AWT_i; \dfrac{AWT_i + AWT_{i+1}}{2}; \dfrac{AWT_i + AWT_{i+1}}{2}\right] \text{ for i} = 1 \\ B_i = \left[AWT_i; \dfrac{AWT_{i-1} + AWT_i}{2}; \dfrac{AWT_i + AWT_i}{2}\right] \text{ for i} = 8 \end{cases} \tag{21}$$

2.4. Validation of the numerical modeling

In order to ensure that the results obtained from simulating the mathematical model accurately reflect reality, it is essential to perform a rigorous validation. The validation of simulations requires experimental data for comparison; however, conducting experiments on the valve that precisely replicate the real conditions of our study proves to be particularly challenging. Indeed, the thermal and mechanical phenomena to which the valve is subjected in an actual operating environment are difficult to reproduce in a laboratory setting. To surmount this difficulty, geometric dimensions, boundary conditions of the exhaust valve are reproduced using the data provided in [21,49].

Fig.14 presents a comparison between the experimental data (shown as dashed lines) and the results of the present study (shown as solid lines). Temperature comparisons were carried out at four points: point 1 at the center of the combustion face, point 2 at the port region, point 3 at the guide level, and point 4 at the tip area. The results show a very good agreement between the numerical and the experimental data, confirming the reliability of the developed model.

2.5. Key methodological consideration and advances over prior work

In principle, a fully coupled thermo-fluid-solid simulation could provide a more detailed representations of the valve heat transfer process, particularly in capturing transient effect during valve opening and closing. However, such an approach requires substantially higher computational resource and is often difficult to integrate into cyclic thermo-mechanical analyses.

The Table 3 below succinctly summarizes the aspects and the factors considered in methodology and, crucially, delineates the specific advantages this offers over previous studies namely, enhanced geometric resolution, the elimination of unphysical boundary condition discontinuities, and ultimately, a demonstrable improvement in prediction accuracy, as validated against experimental data.

3. Application to the exhaust valves mounted on 5.9 l diesel engine

In this study, the adopted methodologyis applied to the exhaust valve of a 5.9 L engine. Initially, essential thermodynamic parameters were determined using the 1D Ricardo Wave model(Low fidelity numerical work), which simulates both turbocharged and naturally aspirated diesel engine configurations. Then, the calculated HTC and AWT are integrated into a finite element simulation using ANSYS(High fidelity numerical work), where the geometry will be created, the mesh will be generated, and a 2D simulation will be performed.

3.1. Geometry of valve

The exhaust valve is characterized by a set of essential technical specifications. In particular, the maximum lift playing a crucial role in regulating exhaust flow and enhancing combustion efficiency which is a key parameter. Additionally, dimensions such as the valve diameter, and stem length, along with other mechanical specifications, help improve its performance under tough conditions. The Table 4 summarizes aforementioned technical parameters of the exhaust valve.

3.2. Model of the diesel engine

The engine used in this study is a turbocharged 5.9 L, six-cylinder diesel engine [50] with 12 exhaust's valves. Table 5 summarizes its

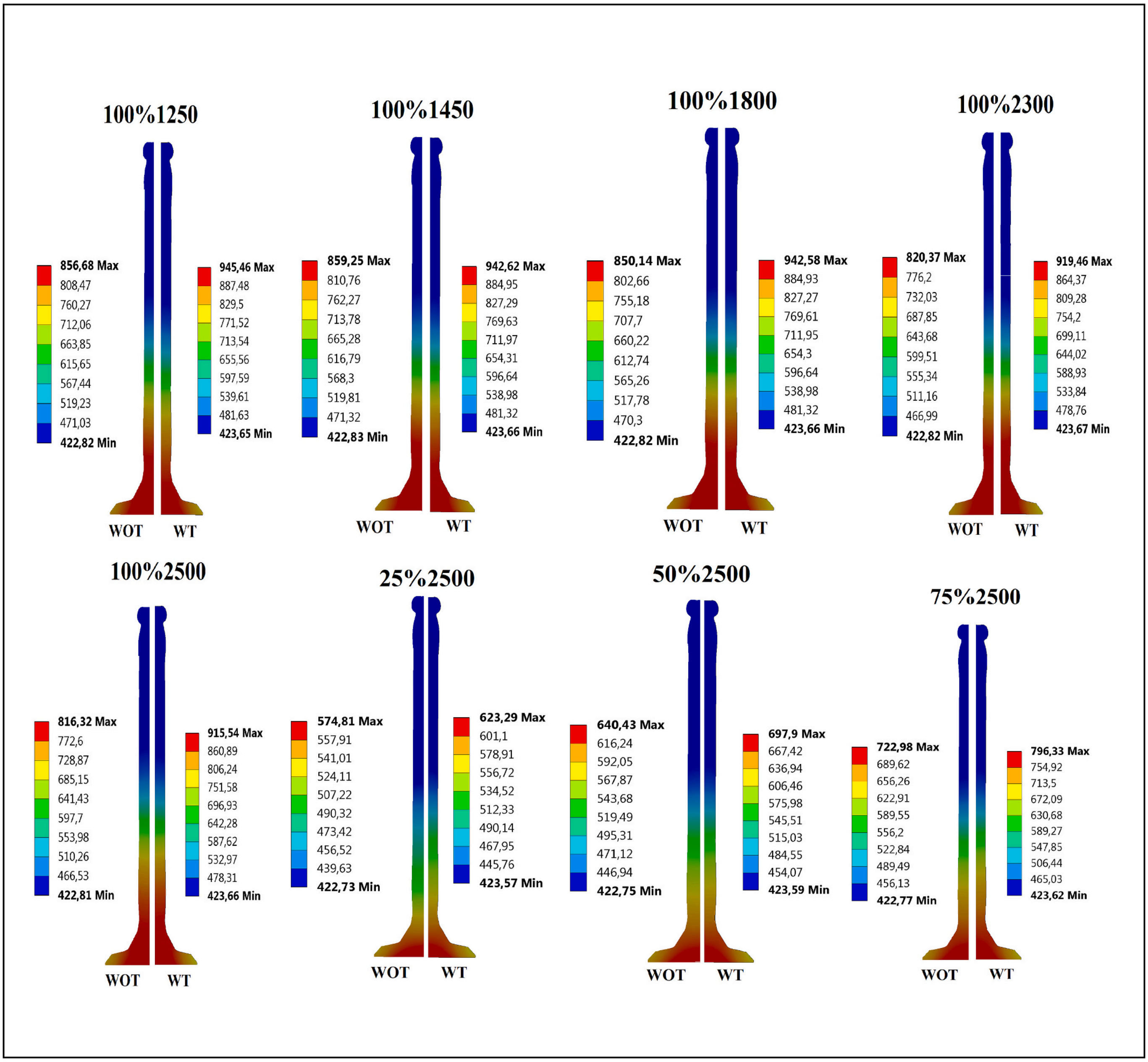

Fig. 24. Temperature maps at various loads and speed in both WT and WOT.

main parameters.

To simulate the gas dynamics of a 5.9 L diesel engine equipped with the Holset Hx35w turbocharger (Fig.15a)a one-dimensional model was developed using the previously validated WAVE model [50].

The 1D WAVE model was initially validated against experimental results [51], demonstrating high accuracy at the point 2500 rpm, 100 % load, with relative errors of less than 1 % for brake power and under 3 % for brake torque, thereby confirming its reliability in capturing transient engine parameters(Fig. 16).

To isolate the effect of turbocharging, the air intake system is modified by removing the turbine and compressor, converting the engine to a naturally aspirated configuration(Fig.15b). All other components were left unchanged, ensuring that the only alteration was the removal of the turbocharger.To regulate the fuel quantity, the same air-fuel ratio as in the turbocharged case is maintained for each engine speed and load condition. The air mass flow rate is first estimated with the turbocharger removed, and then, by keeping this ratio constant, the corresponding fuel quantity is determined to be introduced into Ricardo WAVE model, thus, providing the distribution required thermodynamic parameters.

Indeed, these parameters vary depending on several factors, including engine speed and load. To account for the full range of operating conditions of the diesel engine, four load levels (100 %, 75 %, 50 %, and 25 %) are analyzed across different engine speeds, ranging from 950 rpm to 2500 rpm. The pressure and temperature parameters in the cylinder, as well as the mass flow rate and temperature in the exhaust system, represented in the (Fig.17), correspond to an engine speed of 2500 rpm anda load of 100 % for both naturally aspirated and turbocharged engine.

The evolution of cylinder pressure as a function of crankshaft angle shows notable differences between a naturally aspirated engine and a turbocharged engine(Fig.17a).In a naturally aspirated engine, the peak cylinder pressure is generally lower since air intake relies entirely on atmospheric pressure and the intake flow effect generated by the piston

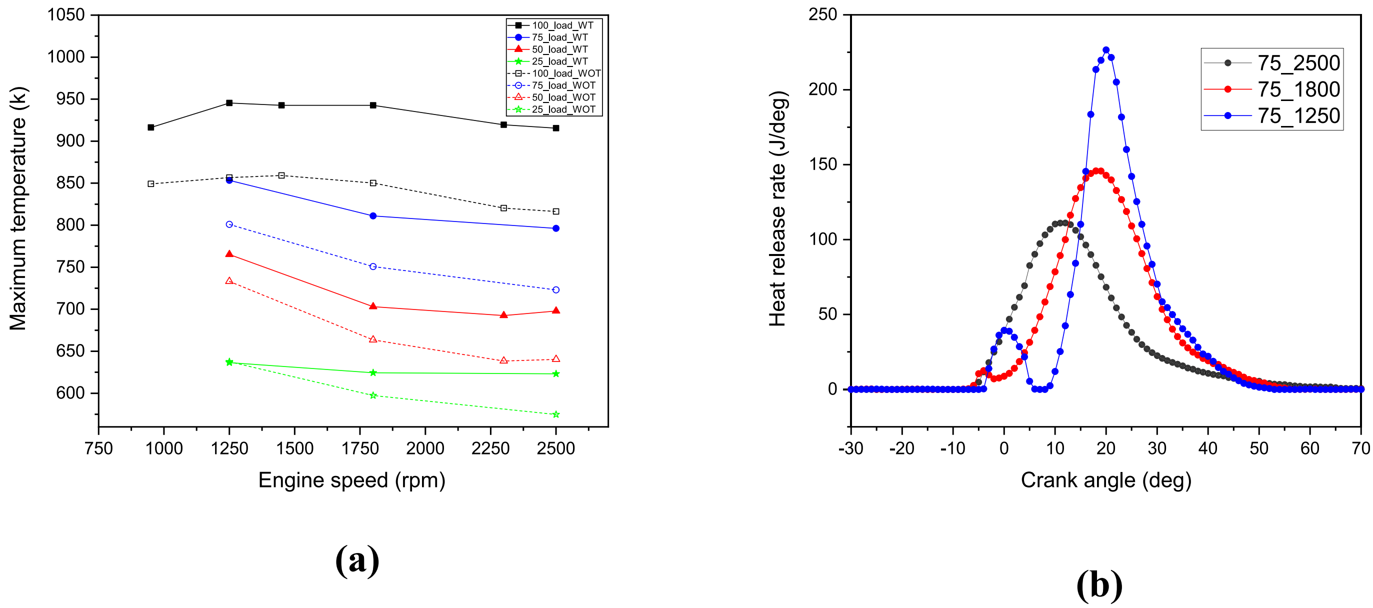

Fig. 25. (a) Maximum temperature at various speeds and (b) Heat release rate at load 75 %.

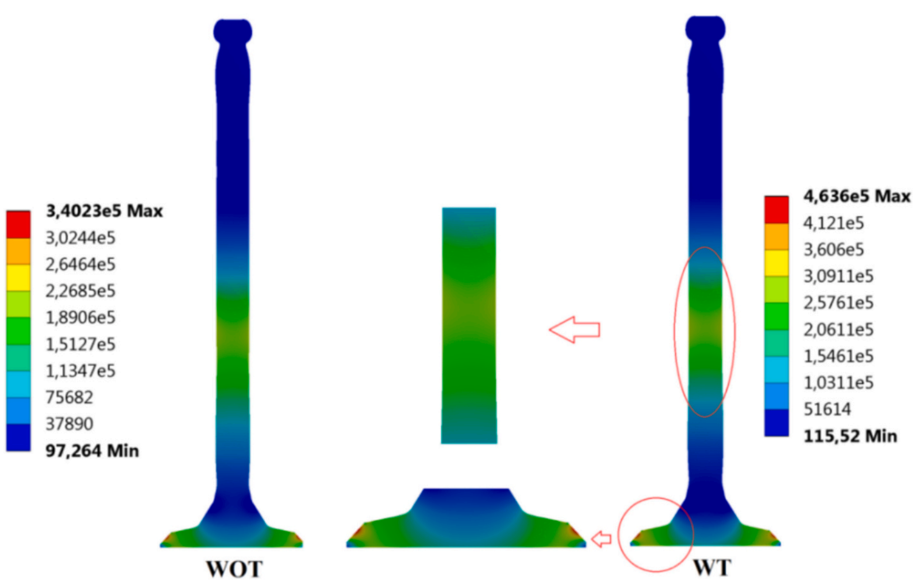

Fig. 26. Heat fluxes through the exhaust valve WT vsWOT.

during the intake stroke. Consequently, the pressure gradually increases during compression, reaches a peak after fuel injection and combustion, and then decreases during the expansion and exhaust phases.In contrast, in a turbocharged engine, the pressure at the beginning of the cycle is significantly higher due to pressurized air intake, which allows a greater mass of air to enter the cylinder. This boost pressure leads to a more intense combustion, resulting in higher peak pressure and temperature (Fig.17b) after ignition compared to a naturally aspirated engine. The **Fig.17c**and Fig.17d show an increase in exhaust gas flow rate and temperature in the turbocharged engine, particularly during the exhaust phase.

3.3. Effect of the turbocharging on Averagethermal boundary conditions

a. **In term of average HTC**

HTCs were calculated for the first five valve zones in both WT andWOT engines using **Eq. 3.** Turbocharging amplifies HTC sensitivity to engine load (Fig. 18)by altering inlet, in-cylinder, and exhaust gas flows, with effects intensifying at higher loads.For the combustion face (Fig. 18a), HTC rises linearly with engine speed in both configurations, but the slope is steeper for WT case. This results from the Woschni model's dependence on piston speed (proportional to RPM) and combustion pressure (elevated under load), where even moderate increases significantly boost HTC.The valve seat (Fig.18b) is predominantly load-sensitive. During valve closure, conduction dominates heat transfer, and seat pressure governs HTC. WT configuration shows linear HTC growth at 25 % load but shift to polynomial trends at higher loads.In cavity, port, and port/guide zones (Fig. 18c-e), HTC varies linearly with load. The slope for WT is nearly double that of WOT, attributed to exhaust gas velocity increases at higher engine speeds.

b. **In term of average AWT**

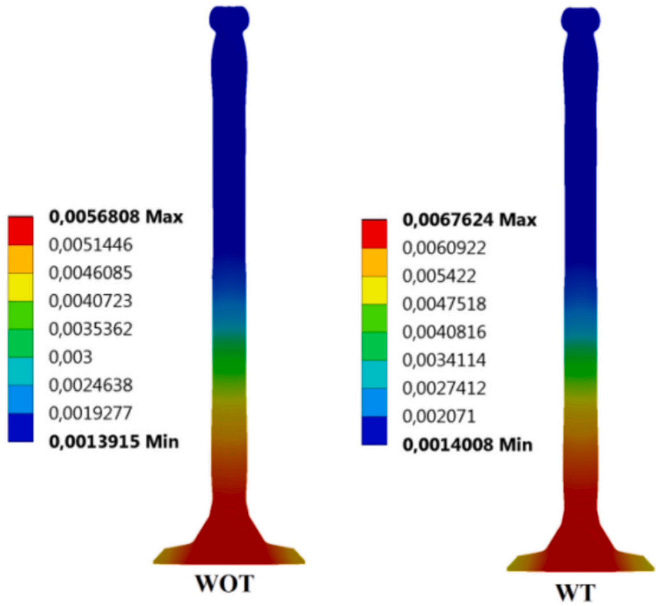

Fig. 27. Thermal expansion map exhaust valve WT vs WOT.

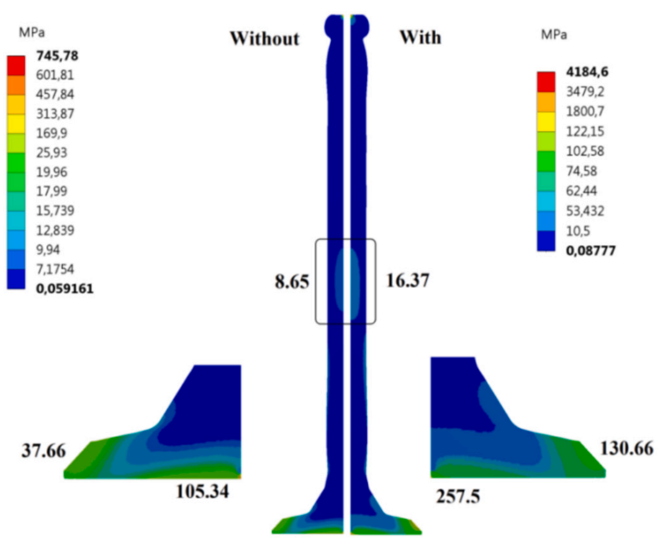

Fig. 28. Distribution of stress intensity through an exhaust valve WT vs WOT.

Adiabatic Wall Temperature (AWT) decreases with lower engine loads in both WT and WOT configurations across most valve zones (Fig. 19). On the combustion face (Fig. 19a), AWT consistently declines as engine speed rises for all loads (100 %–25 %) due to reduced combustion time, leading to incomplete fuel burning and lower peak temperatures.Similar trends occur in the cavity, port, and port/guide zones at ≤75 % load. However, at 100 % load, AWT in these zones peaks at 2300 rpm before declining.

The valve seat (Fig. 19b) shows the strongest turbocharging effect:

- At 75 % load, WT increases AWT by 13.5 K (1250 rpm) → 23 K (1800 rpm) → 29.5 K (2500 rpm).
- This results from higher HTC during peak gas temperatures **(Eq. 3)**, where the product $h(t)\cdot T_a(t)$ amplifies weighted contributions to mean AWT (T_a).

c. **In term of average mechanical loadings**

To achieve a realistic thermo-mechanical model of the valve, the mechanical boundary conditions are defined according to the actual loads. The (Fig.20) illustrates the variation of the spring force as a function of the valve lift. In the closed position, the spring exerts a force of 114 N, sealing the valve against its seat. As the cam lifts the valve, the spring compression increases, reaching a maximum force of 600 N at maximumlift. This behavior is crucial to maintain valve-cam contact, thus preventing valve float at high engine speeds. The results also show that the spring force is independent of turbocharging, since it is determined only by the initial compression force $F_{s,0}$, the stiffness K, and the cam geometry which defines the valve lift L_v (see **Eq.18**). These mechanical parameters remain unchanged for both configurations, while turbocharging mainly affects the thermodynamic conditions of the gases.The average pressure in the port area is presented in **(**Fig.20d**)**.The pressure alters similarly for both configurations, WT and WOT, rising with load and engine speed. The average pressure applied to the valve seat exhibits the same trend as the port pressure, with the maximum value achieving 1.08 bar at 100 % load and 2500 rpm, and enhancing to 1.56 bar whenturbocharging is added.The figure displaying the reaction force at the valve seat indicates a maximum value of approximately 10,000 N when the valve is in the closed position and doubling when the turbo is added.

Table 8
1.6 L Diesel engines specification.

Components	Value
Bore	78.1 mm
Stroke	82.0 mm
Compression Ratio	22.0:1
Firing Order	1–3–4-2
Speed Range	1000–5000 rpm
Fueling	Cylinder injection

Table 7
HTC's established correlations.

Zones	Correlations	Mean Relatif error (%)	Maximum error (%)
Combustion face	$HTC_{WT} = 2.0190\left(\frac{N_{WOT}}{N_{wot_{max}}}\right)^{0.2568}\left(\frac{L_{WOT}}{L_{wot_{max}}}\right)^{0.4296}\left(\frac{P_{WOT}}{P_{wot_{max}}}\right)^{-0.1733}HTC_{WOT}$	2.97	8.75
Seat	$HTC_{WT} = 1.3369\left(\frac{N_{WOT}}{N_{wot_{max}}}\right)^{0.1000}\left(\frac{L_{WOT}}{L_{wot_{max}}}\right)^{0.1648}\left(\frac{P_{WOT}}{P_{wot_{max}}}\right)^{-0.0538}HTC_{WOT}$	1.05	3.31
Cavity	$HTC_{WT} = 1.6295\left(\frac{N_{WOT}}{N_{wot_{max}}}\right)^{-0.1275}\left(\frac{L_{WOT}}{L_{wot_{max}}}\right)^{-0.2331}\left(\frac{P_{WOT}}{P_{wot_{max}}}\right)^{0.0891}HTC_{WOT}$	1.83	4.68
Port	$HTC_{WT} = 2.0008\left(\frac{N_{WOT}}{N_{wot_{max}}}\right)^{0.4651}\left(\frac{L_{WOT}}{L_{wot_{max}}}\right)^{0.2361}\left(\frac{P_{WOT}}{P_{wot_{max}}}\right)^{-0.0039}HTC_{WOT}$	3.61	9.60
Port_guide	$HTC_{WT} = 1.7571\left(\frac{N_{WOT}}{N_{wot_{max}}}\right)^{0.3692}\left(\frac{L_{WOT}}{L_{wot_{max}}}\right)^{0.0746}\left(\frac{P_{WOT}}{P_{wot_{max}}}\right)^{0.1688}HTC_{WOT}$	1.90	5.07

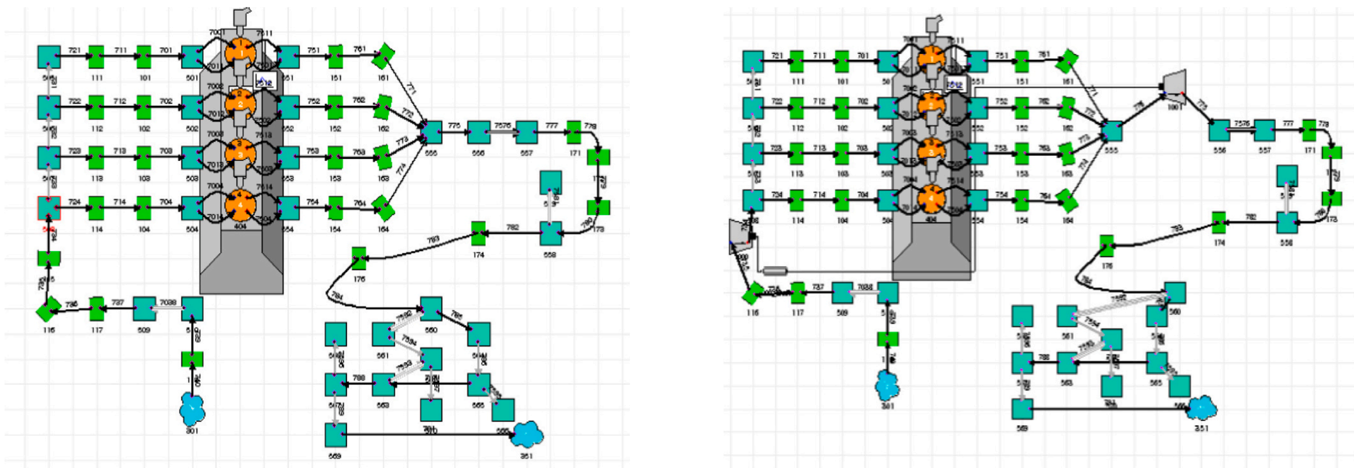

(a) (b)

Fig. 29. 1D wave tested model for(a) Naturally aspirated and (b) Turbocharged engine.

Table 9
Results of the proposed correlations for the tested engine.

Zones	HTC_{WOT}	*Calculated* HTC_{WT}	*Estimated* HTC_{WT}	Relatif Error (%)
Combustion face	334,01	447,7	426,8	4,61
Seat	1265,99	1409,6	1416,7	0,51
Cavity	132,5	168,1	156,5	6,94
Port	192,65	265	250,2	5,60
Port_guide	154,81	190,6	196,4	3,07

3.4. Finite-element modeling

Unsteady heat conduction coupled with structural analysis is solved using the finite element method (FEM) in ANSYS. This approach enables the evaluation of stress and deformation under applied thermal and mechanical loads. By using this method, the structural behavior of the component can be accurately analyzed, ensuring a reliable assessment of its mechanical integrity. In addition and due to its revolution geometry around the vertical axis, the exhaust valve possesses axial symmetry, allowing a full three-dimensional model to be replaced by a two-dimensional axisymmetric one.

a. **Mesh Generation**

Finer mesh is applied in areas of high stress or rapid result variation to ensure better accuracy. ANSYS's automatic meshing tool helps optimize this process while ensuring mesh quality for reliable analysis. The mesh is refined in the seat area, where there is a high heat flux, to capture the thermal gradients more accurately **(**Fig.21**).**To ensure the independence of the results from spatial discretization, a mesh sensitivity study is conducted using the standard grid-convergence index (GCI), in which three different sets of grids, fine (32,773 nodes), intermediate (14,753 nodes) and coarse (3829 nodes) were considered to calculate the temperature at three critical zone Combustion face, Seat and Stem of the valve. The errors results for each mesh are presented inthe Table 6**.**The equations applied in this calculation are described in the work of Cerdoun et al. [22].

b. **Profile of actual boundary conditions**

The results presented here are derived from the application of variable boundary conditions, based on the method described in previous sections. They include AWT and HTC profiles generated using specific functions for each subdivision of the valve. These curves are displayed on the same graph to allow comparison with results obtained under constant boundary conditions, where fixed values of AWT and HTC were applied uniformly across all subdivisions **(**Fig.22**).**This variable boundary condition approach uses smooth transition functions to avoid abrupt changes between regions, leading to continuous HTC variations along the valve surface. Compared to the constant approach, this method enhances the accuracy of the thermal simulation by better representing the local behavior of heat transfer. (See Fig. 23.)

Fig. 23 illustrates the spatial evolution of the variable boundary conditions applied to the valve. On the left, the HTC profile highlights a continuous variation across the subdivisions, indicating a well-controlled thermal transition. The AWT distribution, shown on the right, follows a smooth progression that aligns with the predefined functions.

3.5. Temperature map of the exhaust valve under configurations WT and WOT

Temperature distribution results for engine loads and across engine speeds are shown in **(**Fig.24**)**, for both WT and WOT configurations.In all examined cases, the highest temperature is observed at the combustion face, due to its direct exposure to the heat generated by the combustion process, and is partially cooled in the seat area due to the heat transfer from the circulating coolant.The valve temperature gradually decreases as one moves away from this zone, reflecting the attenuation of heat as it dissipates toward other parts of the engine.

The temperature distribution follows a similar trend in both (WT) and (WOT) configurations, with peak values observed at 100 % load across all valve regions. This distribution progressively decreases with reduced engine loads of 75 %, 50 %, and 25 %.

The effect of the turbocharger on the valve temperature becomes more significant as speed increases, which is quantified for 100 % load by a temperature difference reaching 100 K at 2300 and 2500 rpm, while,it decreases to 92 K and 89 K at 1800 and 1250 rpm, respectively.

This can be explained by the fact that at high engine speeds and load, the rise in exhaust gas temperature and mass flow rate increases the energy available at the turbine inlet. This additional energy raises the turbocharger's rotational speed, which in turn improves the compression of the intake flow. This mechanism confirms that the effect of the turbocharger on the valve temperature becomes more noticeable at high engine speeds.

The maximum temperature for each load and engine speed, for both engine configurations, is presented in (Fig.25a).As engine speed increases, the combustion process in diesel engines undergoes significant changes that impact both the heat release profile and the maximum temperature experienced by engine components such as the exhaust valves. At 1250 rpm, combustion occurs in two distinct phases: a rapid premixed combustion phase followed by a slower diffusion combustion phase, resulting in a high and prolonged heat release (Fig.25b). This leads to higher temperatures at the exhaust valves. At 1800 rpm, these two combustion phases persist but become closer together, with the diffusion phase diminishing in intensity due to the reduced time available for combustion, leading to a decrease in heat transferred to the valves. At 2500 rpm, the time for combustion is so limited that the premixed and diffusion phases merge into a single phase, resulting in a lower total heat release per cycle and, consequently, lower temperatures at the exhaust valves. In addition, as engine speed increases, HTC between the hot gases and the cylinder walls improves, allowing heat to be evacuated more quickly to the cooling system (Fig.18a).

Fig.26 highlights two main zones of heat dissipation: the valve seat and the valve guide. The valve seat, being in direct contact with the cooled cylinder head, constitutes the primary path for heat transfer. This dominant role is attributed to the combination of efficient thermal contact and the high thermal conductivity of the materials employed, which explains the peak heat flux observed in this region reaching a maximum value of 463 kW/m^2 in the turbocharged case and 340 kW/m^2 in the naturally aspirated case. In contrast, the valve guide shows a significantly lower heat flux on the order of 240 kW/m^2 in the turbocharged configuration and 160 kW/m^2 in the naturally aspirated configuration due to the presence of a lubricating oil film and a reduced contact surface, which together hinder conduction [41].However, this part still plays a notable role in the overall heat dissipation [27,48], contributing to the temperature distribution along the stem and indirectly affecting thermal expansion and the resulting mechanical stresses.

In Fig.27, the thermal expansion of the valve is compared at the two engine configurations. In a turbocharged engine, the high temperature of the burnt gases causes greater expansion of the valve, especially at the head, which is directly exposed to the hot gas flow. In contrast, in WOT case, the temperature rise is more moderate, thus limiting thermal expansion. At the guide, expansion remains very low, the proximity of the metal cylinder head and the contact with oil ensure effective heat dissipation, preventing significant deformation [52]. Near the seat, cooling by liquid or by the metal mass of the seat creates a thermal gradient that slightly reduces expansion in that area.

Fig.28 shows the distribution of the stress equivalent Von Mises at the load 75 % for the speed engine of 2300 rpm for both engines. The maximum Von Mises stresses are mainly concentrated in three zones of exhaust valve combustion face, seat and guide. The most critical is the combustion valve with reaches 105 MPa in WOT case and increase to 257.5 MPa in the turbocharged one which is directly exposed to high pressure of combustion gases. The second is the valve seat which experiences high mechanical stresses (about 130 MPa in the WT configuration) especially during valve closure and is affected by thermal gradient exchange and high reaction force. In these cases studies, all these values of stresses are less than 400 MPa, the yield strength of the exhaust valve material.

4. Deduction of HTC'scorrelations for exhaust valve's turbocharged engine

In the thermal analysis of exhaust valves, the HTC is a critical parameter in ICE. However, the thermodynamic properties of combustion and exhaust gases including pressure, temperature and velocity are not always available for all engines, particularly in the case of performance improvement with the addition of a turbocharger.

This study aims to develop a mathematical correlation to estimate HTC in different zones of the exhaust valve, based on the characteristics of the same engine non-turbocharged. The developed correlation is based on the integration of engine variables such engine speed (N), load (L), power (P), and the HTC of the non-turbo engine:

$$HTC_{WT} = f\left(HTC_{WoT}, Power_{WOT}, Speed_{Engine_{wot}}, Load_{Engine_{wot}} \right) \tag{21}$$

The correlation model established by this paper based on these previously cited variables and several constants is the following is used for the 5 zones of the valve is the following:

$$HTC_{WT} = A\left(\frac{N_{WOT}}{N_{wot_{max}}}\right)^{a}\left(\frac{L_{WOT}}{L_{wot_{max}}}\right)^{b}\left(\frac{P_{WOT}}{P_{wot_{max}}}\right)^{c} HTC_{wot} \tag{22}$$

The determination of the constants A, a, b, c and d was carried out for each valve zone using the HTC values evaluated in the previous sections, for both cases: with and without turbocharger. For each correlation these coefficients were determined using 16 cases for both engines for a speed range of 950 to 2500 and for four loads 100, 75, 50 and 25. The obtained correlations are summarized in the following Table 7.

To test the proposed correlations, a 1D engine model (1.6 L, 4 cylinders, 4 strokes, Diesel) in which the engine specification are summarized in Table 8, was used to simulate both a turbocharged engine (Fig.29a) and a naturally aspirated engine (Fig.29b). The heat transfer coefficients HTC_{WT} and HTC_{wot} were calculated accordingly using the proposed approach. Alternatively,HTC_{WT} was evaluated by applying the correlations for the application case corresponding to an engine speed of $N_{WOT} = 2500$ rpm, a power $P_{WOT} = 23,55\ kw$, and a load of $L_{WOT} =$ 50%, developed for each zone of the exhaust valve.The results are summarized in the Table 9 and indicate that the relative errors between the calculated and predicted values remain below 7 %. These results confirm that the proposed correlations provide a satisfactory estimation of the thermal boundary conditions for a turbocharged engine.

5. Conclusion

Based on the comprehensive results presented in the study, the following conclusions are drawn regarding the thermomechanical behavior of exhaust valves in turbocharged diesel engines:

1. **Turbocharging significantly elevates thermal and mechanical loads on exhaust valves.** The integration of a turbocharger increases peak valve temperatures by up to 100 K at high-load/high-speed conditions (100 % load, 2500 rpm), primarily due to higher exhaust gas temperatures and mass flow rates. This thermal intensification is most pronounced on the combustion face, which experiences direct exposure to combustion gases. Mechanically, Von Mises stress at the combustion face surges by 144 % (from 105.34 MPa in WOT caseto 257.5 MPa in WT configurations at 2300 rpm, 75 % load). Heat flux at the valve seat also rises by 36 % (463 kW/m^2 vs. 340 kW/m^2), while the reaction force at the seat doubles during valve closure.
2. **Heat transfer coefficients (HTC) are highly sensitive to turbocharging and operating conditions.** The HTC increases linearly with engine speed and load across all valve zones, but turbocharging steepens this trend. The combustion face HTC exhibits the strongest speed dependence (+256 % sensitivity), while the seat zone is predominantly load-driven. In port/guide zones, turbocharging nearly doubles HTC slopes compared to naturally aspirated engines. Adiabatic wall temperature (AWT) behavior varies by zone: it decreases with speed on the combustion face due to reduced combustion completeness but increases at the seat under high loads due to weighted thermal contributions.

3. **Novel correlations enable accurate prediction of turbocharged HTC using naturally aspirated engine data.** The study establishes valve zone-specific correlations (Table 5, Eq. 22). These equations, requiring only engine speed (N), load (L), and power (P) inputs, predict turbocharged HTC with <4 % mean error (validated against a separate 1.6 L engine model, Table 7). This eliminates the need for exhaustive thermodynamic data during turbocharger integration.
4. **Critical failure zones are identified through spatial analysis.** The combustion face endures the highest temperatures and stresses (Fig. 24–25). The valve seat experiences peak heat flux (Fig. 26) and mechanical stress during closure (10,000 N reaction force, Fig. 20). Thermal expansion is most severe at the valve head in turbocharged engines (Fig. 27), though stresses remain below the material yield strength (400 MPa).
5. **Practical implications inform engine design.** Turbocharging exerts its most severe impacts at high speeds (>1800 rpm) and loads (75–100 %). The proposed correlations offer engineers a rapid tool to assess thermal risks during turbocharger retrofits, guiding material selection and cooling optimizations. By quantifying how turbocharging amplifies valve thermo-mechanical loads, this study provides critical data for enhancing durability in high-performance diesel engines.

CRediT authorship contribution statement

Fatiha Sahi: Writing – original draft, Validation, Methodology, Investigation, Formal analysis, Data curation, Conceptualization. **Mahfoudh Cerdoun:** Writing – review & editing, Writing – original draft, Validation, Supervision, Methodology, Investigation, Formal analysis, Data curation, Conceptualization. **Youcef Sehili:** Writing – review & editing, Methodology. **Mohammed Amine Elhameur:** Writing – review & editing, Methodology. **Lyes Tarabat:** Writing – review & editing. **Carlo Carcasci:** Software, Formal analysis, Conceptualization.

Declaration of competing interest

The authors have no relevant financial or non-financial interests to disclose.

Data availability

Data will be made available on request.

References

[1] J.B. Heywood, Internal Combustion Engine Fundamentals, McGraw-Hill, 1988 (International Editions).
[2] C.R. Ferguson, A.T. Kirkpatrick, Internal Combustion Engines, 2nd ed, Wiley, New York, 2001.
[3] A.C. Alkidas, Intake-Valve Temperature and the Factors Affecting It, SAE Paper 971729, 1997.
[4] HeislerH., Advanced Engine Technology, Society of Automotive Engineers, Hodder Headline Group, London, 1995.
[5] L.C. Yang, A. Hamada, K. Ohtsubo, Engine Valve Temperature Simulation System, SAE Paper 2000–0100564, 2000.
[6] R.D. Cook, Finite Element Modeling for Stress Analysis, Wiley, New York, 1995.
[7] J.M. Cherrie, Factors Influencing Valve Temperatures in Passenger Car Engines, SAE Paper 650484, 1965.
[8] R.P. Worthen, D.G. Rauen, Measurement of Valve Temperatures and Strain in a Firing Engine, Technical Paper 860356, 1986, pp. 625–637. J. R.
[9] F. Lai, S. Qu, Y. Duan, et al., The wear and fatigue behaviours of hollow head & sodium filled engine valve, Tribol. Int. 128 (2018) 75–88.
[10] K. Goudarzi, M.H. Shojaefard, M. Fazelpour, Effect of contact pressure and frequency on contact heat transfer between exhaust valve and its seat, Int. J. Eng. Trans. B 21 (4) (December 2008).
[11] A. Stotter, K.S. Woolley, Exhaust valve temperature a theoretical and experimental investigation, SAE Trans. 74 (1966) 89.
[12] C. Federico, L. Cesar, R. Jose, Z. Fernando, C. Alberto, Numerical and Experimental Stress Analysis of an Internal Combustion Engine Valve During the Closing Event, Proc. Inst. Mech. Eng., Part D: J. Automob. Eng. 228 (5) (2014) 479–489.
[13] L. Witek, Failure and thermo-mechanical stress analysis of the exhaust valve of diesel engine, Eng. Fail. Anal. 66 (2016) 154–165.
[14] T. Sanoj, S. Balamurugan, Thermo mechanical analysis of engine valve, Int. J. Sci Res. 3 (5) (2014) 1834–1838.
[15] A. Zemmouri, S. Azzouz, D. Benchadli, A. Ayad, Study of the periodic thermal contact between exhaust valve and its seat in an internal combustion engine, Maint. Reliab. 25 (2) (2023) pp.
[16] M. Hazra, A. Sambasiva Rao, A.K. Singh, Corrosion fatigue failure of exhaust valve of a diesel generator, J. Fail. Anal. Prev. 23 (4) (2023) 1402–1412.
[17] M. Chavoushi, A. RaisiNafch, Stress analysis by finite element method in the exhaust valve without coating and with silicon nitride ceramic coating in a two-stroke diesel engine, Modares Mech. Eng. 24 (11) (2024) 71–77.
[18] Z. Deng, F. Lan, et al., The research on thermal-mechanical coupled analysis and the lightweight Design of Engine Exhaust Valve, Appl. Mech. Mater. 729 (2014).
[19] Deng, L. Huang, M. Xin, Numerical analysis of valve structure of high power marine engine, Brodogradnja 72 (2) (2021) 115–126.
[20] G. Woschni, A Universally Applicable Equation for the Instantaneous Heat Transfer Coefficient in the Internal Combustion Engine, SAE Technical Paper, 1967.
[21] R. Prasad, N.K. Samria, Transient heat transfer studies on a diesel engine valve, Int. J. Mech. Sci. 33 (1991) 179–195.
[22] M.H. Shojaefard, A.R. Noorpoor, D.A. Bozchaloe, et al., Transient thermal analysis of engine exhaust valve, Numer. Heat Transf. Part A Appl. 48 (2005) 627–644.
[23] M. Cerdoun, C. Carcasci, A. Ghenaiet, An approach for the thermal analysis of internal combustion engines' exhaust valves, Appl. Therm. Eng. 102 (2016) 1095–1108.
[24] M. Cerdoun, C. Carcasci, A. Ghenaiet, Analysis of unsteady heat transfer of internal combustion engines'exhaust valves, Int. J. Engine. Res. 19 (2018) 613–630.
[25] M. Cerdoun, S. Khalfallah, A. Beniaiche, et al., Investigations on the heat transfer within intake andexhaust valves at various engine speeds, Int. J. Heat Mass Transf. 147 (2020) 119005.
[26] M. Cerdoun, B. Fersaoui, S. Khalfallah, Effect of the engine speed and loading on the heat transfer within exhaust valves, in: E3S Web of Conferences vol. 128, EDP Sciences, 2019, p. 01001.
[27] B. Fersaoui, M. Cerdoun, A. May, C. Carcasci, Thermo-mechanical stress analysis within a steel exhaust valve of an internal combustion engine, Proc. Inst. Mech. Eng. C J. Mech. Eng. Sci. 236 (1) (2022) 635–654.
[28] S. Wang, J. Liu, X. Xia, Y. Wang, Y. Lin, Effect of Turbocharging System on the Performance of a Gasoline Engine, Hunan University, 15 Apr 2011, pp. 5882–5885 (IEEE).
[29] J. Zareei, S. Ahmadipour, The effect of the turbocharger system and different fuels on the performance and exhaust emissions of a diesel engine by a numerical study, Int. J. Automot. Eng. 10 (2) (2020) 3295–3310.
[30] M.A. El Hameur, M. Cerdoun, L. Tarabet, An improved model for primary prediction of performance map for turbocharger radial turbine, Proc. Inst. Mech. Eng., Part D: J. Automob. Eng. 239 (8) (2024) 3557–3578.
[31] M.A. El Hameur, Y. Sehili, M. Cerdoun, L. Tarabet, G. Ferrara, An approach to select an appropriate turbocharger for matching with an internal combustion engine, Int. J. Engine Res. 24 (5) (2023) 2072–2090.
[32] Y. Sehili, L. Tarabet, M. Cerdoun, C. Lacroix, Toward improving efficiency and mitigating emissions in a natural gas/diesel direct injection dual fuel engine using EGR, Int. J. Engine Res. 25 (11) (2024) 1976–1990.
[33] Y. Sehili, M. Cerdoun, K. Loubar, L. Tarabet, Dual fuel engine injector temperature monitoring: an innovative thermal analysis approach, Appl. Therm. Eng. 249 (2024) 123370.
[34] Z. Lin, S. Liu, Q. Sun, Y. Qi, Z. Wang, J. Li, Effect of injection and ignition strategy on an ammonia direct injection–hydrogen jet ignition (ADI-HJI) engine, Energy 306 (C) (2024) 132451.
[35] Z. Feng, W. Chenghao, F. Jianqin, L. Jingping, D. Xiongbo, S. Zhiqiang, Abnormal combustion and NOx emissions control strategies of hydrogen internal combustion engine, Renew. Sust. Energ. Rev. 219 (September 2025) 115847.
[36] C. Ali, Y. Ha-Jun, L. Joo-Sung, A. Tesfalem, Z. Mohamadamin, S. Sangwon, W. John, L. Chul-Jin, Unlocking low-carbon hydrogen transportation through a cost-effective hybrid CO2/heat looping strategy, Renew. Sust. Energ. Rev. 219 (September 2025) 115848.
[37] C.A. Finol, K. Robinson, Thermal modelling of modern engines: a review of empirical correlations to estimate the in-cylinder heat transfer coefficient, Proc. Inst. Mech. Eng., Part D: J. Automob. Eng. 220 (2006) 1765–1781.
[38] W.J.D. Annand, Heat transfer in the cylinders of reciprocating internal combustion engines, Proc. Instn Mech. Engrs 177 (36) (1963) 973–990.
[39] G. Eichelberg, Some investigations on old combustion engine problems, Engineering 148 (I, II) (1939), 463–466, 547–550.
[40] Kastner LJ, Williams TJ and White J B. Poppet Inlet Valve Characteristics and Their influence on the Induction Process, Pro Instn Mech. Eng., vol. 178, pt. 1, no. 36, pp. 951–978, 1963–196.
[41] S. Song, M. Yovanovich, Relative contact pressure: dependence upon surface roughness and Vickers microhardness, J. Thermophys. Heat Transf. 2 (1) (1988) 43–47.
[42] Yamamoto H, Seki N and Fukusako S. Forced confection heat transfer on heated bottom surface of a cavity, J. Heat Transf.
[43] Bhatti A and Aung W. Finite difference analysis of laminar separated forced convection in cavities. J. Heat Transf., 106(1), 49–54.
[44] Aung W. An interferometricinvestigation of separated forced convection in laminar flow past cavities, ASME J. Heat Transfer.
[45] R.F. Richards, M.F. Young, J.C. Haiad, Turbulent forced convection heat transfer from a bottom heated open surface cavity, Int. J. Heat Mass Transf. 30 (1987) 2281–2290.
[46] R. Chapman, A Theoretical Analysis of Heat Transfer in Regions of Separated Flow, 1956.

[47] C. Carcasci, B. Facchini, A numerical procedure to design internal cooling of gas turbine stator blades, RevueGénérale de Thermique (Int. J. of Thermal Sciences) 35 (April 1996) 257–268, n. 412. Elsevier, (ISSN: 00353159).

[48] S.W. Churchill, M. Bernstein, A correlating equation for forced convection from gases and liquids to a circular cylinder in cross flow, Heat Trans. ASME. Ser. C 99 (1977) 300–306.

[49] N.K. Prasad Rand Samria, Heat transfer and stress fields in the inlet and exhaust valves of a semi-adiabatic diesel engine, Comput. Struct. 34 (5) (1990) 765–777.

[50] Ricardo WAVE 8.0 Wave user Manual. 2025.

[51] https://www.iveco.com>NewEurocargo catalogue.pdf (page 20/27). 2025.

[52] K. Neeraj, R.K. Misra, S. Satpal, Modeling of thermal expansion behavior of densely packed Al/SiC composites, Int. J. Solids Struct. Vol. 102–103 (15 December 2016) 77–88.